Numerical Simulation of the Meso-β Scale Structure and Evolution of the 1977 Johnstown Flood. Part II: Inertially Stable Warm-Core Vortex and the Mesoscale Convective Complex

DA-LIN ZHANG* AND J. MICHAEL FRITSCH

Department of Meteorology, The Pennsylvania State University, University Park, PA 16802

(Manuscript received 27 June 1986, in final form 30 March 1987)

ABSTRACT

A mesoscale warm-core vortex associated with the mesoscale convective complex (MCC) that produced the 1977 Johnstown flood is examined using a three-dimensional nested-grid model simulation of the flood episode. In the simulation, the vortex plays a key role in determining the evolution of the MCC, a squall line, and the distribution of heavy precipitation. The vortex has a space scale of 100–200 km in diameter and a time scale of more than 18 hours. Its low pressure center extends from the midtroposphere down to the surface, and its maximum vorticity occurs between 850 and 700 mb. A pool of cool moist downdraft air develops in the surface to the 850 mb layer beneath the warm core, while a cold dome forms in the vicinity of the tropopause above the warm core. Following forcing from repeated deep convection prior to model initial time, the vortex is initiated by mesoscale ascent associated with a traveling meso-α scale wave. Genesis takes place in a nearly saturated, slightly conditionally unstable environment with weak horizontal deformation and vertical shear. The vortex is then energetically supported primarily by latent heat release from stratiform (resolvable-scale) cloud condensation in the low- to midtroposphere. In the decaying stage, the vortex is maintained by inertial stability. The evolution of the warm-core mesovortex appears to depend upon the concurrent development of deep convection and the mesoscale flow structure. In particular, moist downdrafts play an important role in controlling the strength of the vortex and the amount of resolvable-scale rainfall. Associated with the mesovortex, an intense vertical circulation with strong low-level convergence and upper-level divergence develops. In addition, a strong cyclonic circulation extends to 300 mb where a changeover to anticyclonic circulation occurs. It is found that equivalent potential temperature and the horizontal momentum are nearly uniformly distributed in the immediate environment of the vortex. The resultant weak horizontal deformation provides an important energy-preserving mechanism for the maintenance of the warm-core structure while inertial stability of large tangential winds helps the longevity of the vortex circulation. At upper levels, a mesohigh with strong anticyclonic outflow develops above the vortex. The mesohigh behaves like an "obstacle," forcing the horizontal environmental wind flow around it. To the northeast of the upper level mesohigh, a northwesterly jet streak develops between the strong anticyclonic outflow and a baroclinic zone farther north.

The results suggest that successful prediction of the evolution of mesoscale convective weather systems not only hinges upon the convective parameterization, but also depends upon the model's ability to reproduce the timing and location of resolvable-scale condensation. The resolvable-scale phase changes, and associated latent heat release, strongly affect the mesoscale circulation and contributes about 30% to 40% of the total precipitation from the mesoscale convective systems.

1. Introduction

Following recognition of the mesoscale convective complex (MCC) as a unique type of weather system (Maddox, 1980), much attention has focused on understanding the processes whereby MCCs and other mesoscale convective systems (MCSs) develop, evolve and produce significant rainfall (e.g., see Bosart and Sanders, 1981; Cotton et al., 1983; Maddox, 1983; Wetzel et al., 1983; Perkey and Maddox, 1985; Smull and Houze, 1985; Kane et al., 1987; Fritsch et al., 1986; Leary and Rappaport, 1987). A common thread that seems to be emerging from the many different studies of mesoscale convective weather systems is the realization that *stratiform*[1] clouds and precipitation may have an important impact on the evolution of the predominantly convective systems, and that the stratiform precipitation seems to be related to the appearance or intensification of mesovortices (see Houze, 1977; Houze and Betts, 1981; Gamache and Houze, 1982, 1985; Leary and Rappaport, 1987; Houze and Rappaport, 1984; Smull and Houze, 1985).[2] Based on satellite imagery, Johnston (1981) showed that such vor-

* Present affiliation: National Center for Atmospheric Research, Boulder, CO 80307, which is sponsored by the National Science Foundation.

[1] The term stratiform is used rather loosely here since Leary and Rappaport (1987) have shown that, at least in some instances, the so-called stratiform regions are actually marginally convective. A more appropriate term, from the standpoint of numerical modeling, is "grid-resolvable scale" precipitation.

[2] Mesovortices are defined here as significant concentrations of positive relative vorticity of magnitude at least that of the local Coriolis parameter.

tices develop quite commonly in conjunction with MCCs. The cloud patterns associated with these vortices are typically 100 to 400 km in diameter, persist for a few hours to several days, and form primarily at mid- to low levels. In agreement with this, Maddox (1980, 1983) and Bosart and Sanders (1981) noted what appeared to be mesoscale midtropospheric ascent during the mature stage of MCCs. This midlevel ascent was highly correlated with midlevel cyclonic and upper-level anticyclonic circulations. Leary (1979) also noticed a cyclonic/anticyclonic couplet in her analysis of a tropical weather system, and Houze (1977) and Leary and Houze (1979) noted that there was a sizeable contribution of stratiform precipitation to the total rainfall in the tropical weather systems they investigated. In studies of midlatitude MCCs, Rockwood et al. (1984) and Smull and Houze (1985) provided observational evidence of a relatively large contribution of stratiform precipitation in association with the development of a mesolow and mesovortex. Moreover, Rappaport and Leary (1985) detected midlevel cyclonic spiral bands in an analysis of a midlatitude MCS and Leary and Rappaport (1987) clearly documented the development of a banded cyclonic circulation in the "stratiform" region of an MCC.

The importance of the stratiform or resolvable-scale latent heat release to the development of mesoscale vortices has been investigated in a number of numerical studies of meso-α scale extratropical cyclones, polar lows and tropical storms. For example, Sardie and Warner (1983, 1985) found that the resolvable-scale latent heating greatly enhanced the deepening rates of polar lows. Similarly, Anthes and Keyser (1979) and Anthes et al. (1983) found that the deepening rate of meso-α scale extratropical cyclones is substantially increased if the maximum latent heating occurs at relatively low levels. In numerical models, this is most likely to happen if the latent heating occurs through resolvable-scale circulations and not through convective parameterization. This is because most convective parameterizations implicitly incorporate the effects of vertical eddy transport of heat by convection; this tends to shift the heat released in convective clouds to higher levels (Anthes, 1977), whereas in resolvable-scale condensation no such shift occurs. The effect of changing the level of maximum heating is so strong that in a linear analytic study of the mechanisms of deepening of the *QE II* storm, Gyakum (1983) computed a 24-h central pressure difference of 50 mb when the level of maximum heating was shifted downward by only 200 mb, i.e., from 500 mb down to 700 mb. Likewise, Koss (1976) found that the deepening rate of tropical waves is enhanced if the level of maximum latent heating is lowered. Therefore, there seems to be a strong correlation between mesocyclogenesis (or the rate of deepening) and mid- to low-level heating by stratiform (resolvable-scale) condensation.

Mesocyclogenesis also occurred in the numerical simulation of the squall line and mesoscale convective complex that produced the 19–20 July 1977 Johnstown, Pennsylvania flood (Zhang and Fritsch, 1986a, hereafter referred to as ZF86). Specifically, the numerical model (see Anthes and Warner, 1978; and ZF86) produced a mesoscale midlevel warm-core vortex in conjunction with the mesoscale convective complex. The likelihood that such a warm-core vortex was actually present is supported by Bosart and Sanders' (1981) finding that the MCC responsible for the Johnstown flood became a tropical storm as it moved eastward over the warm water of the Atlantic. Other evidence for the existence of the vortex is that its evolution corresponds well with that of a major mesolow apparent in the surface data (see Hoxit et al., 1978; Bosart and Sanders, 1981; and ZF86). In addition, Figs. 1a and 1b show two barograph traces (Philipsburg and State College, Pennsylvania) that support the existence of the mesolow/vortex. Even though the center of the low passes about 20 to 30 km to the north of these two stations (see Fig. 1c), they still experience about a 2 mb pressure drop within approximately an hour. Figure 1c compares the path of the observed mesolow to the model-simulated path; the timing and location of the mesolow propagation appear to be reproduced well by the model. The mesolow forms in conjunction with the passage of a midlevel short wave and propagates east southeastward with a speed of 6–8 m s^{-1}.

The simulated warm-core vortex/mesolow has a space scale of 100–200 km in diameter and persists more than 18 hours (see ZF86). As the vortex develops, it substantially alters the mesoscale flow fields and the MCC structure, and produces significant precipitation. In Part I of this series of papers (ZF86), the model-simulated surface features, and the low- to upper-level wind, thermal and height fields associated with the mesovortex and MCC are found to conform very well to the observational analyses by Hoxit et al. (1978) and Bosart and Sanders (1981). The objective of this paper is to use the model simulation to examine the meso-β scale structure and evolution of the inertially stable[3] mesovortex and the MCC since the standard upper-air observations are too coarse to resolve the detailed structure. Another objective of this paper is to explore how the development of the mesovortex is related to convective and resolvable-scale processes. The model simulation is presented from a fine-mesh framework since it contains the most detailed information of the meso-β scale structure. In section 2, the evolution of the environmental wind pattern associated with the mesoscale systems is shown. Section 3 describes the vertical and midlevel horizontal structure of the warm-core vortex, the MCC and other related features at different stages of development. Section 4 shows the resolvable-scale precipitation distribution associated with

[3] Inertial stability, defined by $[f + \partial(rv)/r\partial r][f + 2v/r]$, where v is the tangential wind (see Schubert and Hack, 1982), provides resistance to radial displacements such that a mesoscale vortex, once formed, will not quickly decay.

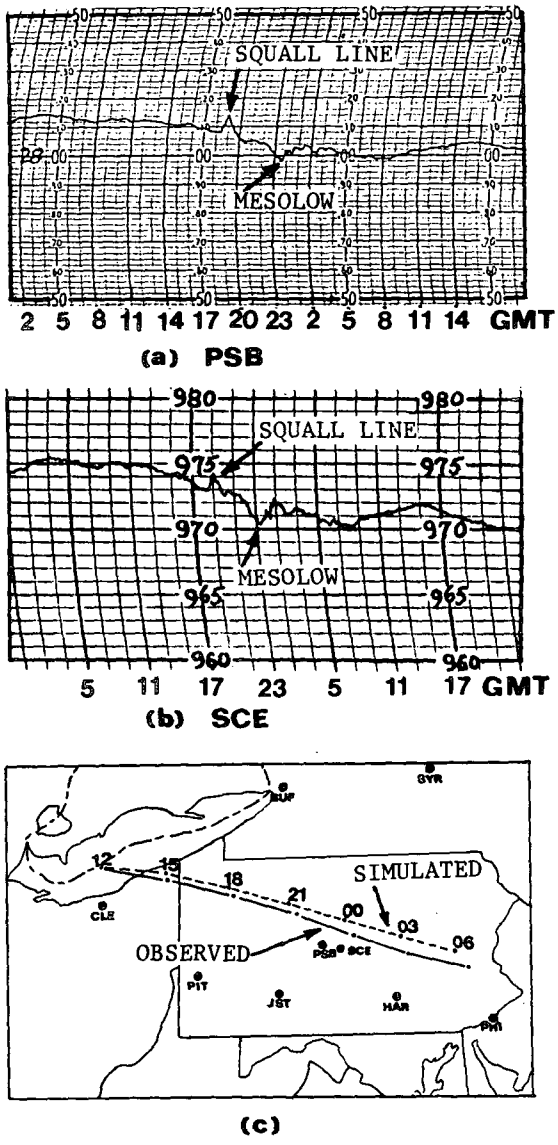

FIG. 1. Portion of 4-day/page barograph traces for (a) Philipsburg (PSB) and (b) State College (SCE), Pennsylvania (see Fig. 1c for locations). The passage of the mesolow and the squall line is labeled on each chart. (c) Comparison of the path of the observed mesolow with the model-simulated path.

the vortex, and provides some discussion of the problems related to numerical prediction of mesolows. The mechanisms whereby the mesovortex forms, intensifies and dissipates are discussed in section 5. The final section summarizes the results and presents some concluding remarks.

2. Evolution of environmental flow

Figure 2 shows the mesoscale flow fields at low (900 mb), middle (500 mb) and upper (300 mb) levels at 1200 UTC 19 July, i.e., at model initial time. Shading denotes the predicted area of active convection at the first time step (see ZF86 for discussion). Based on sat-

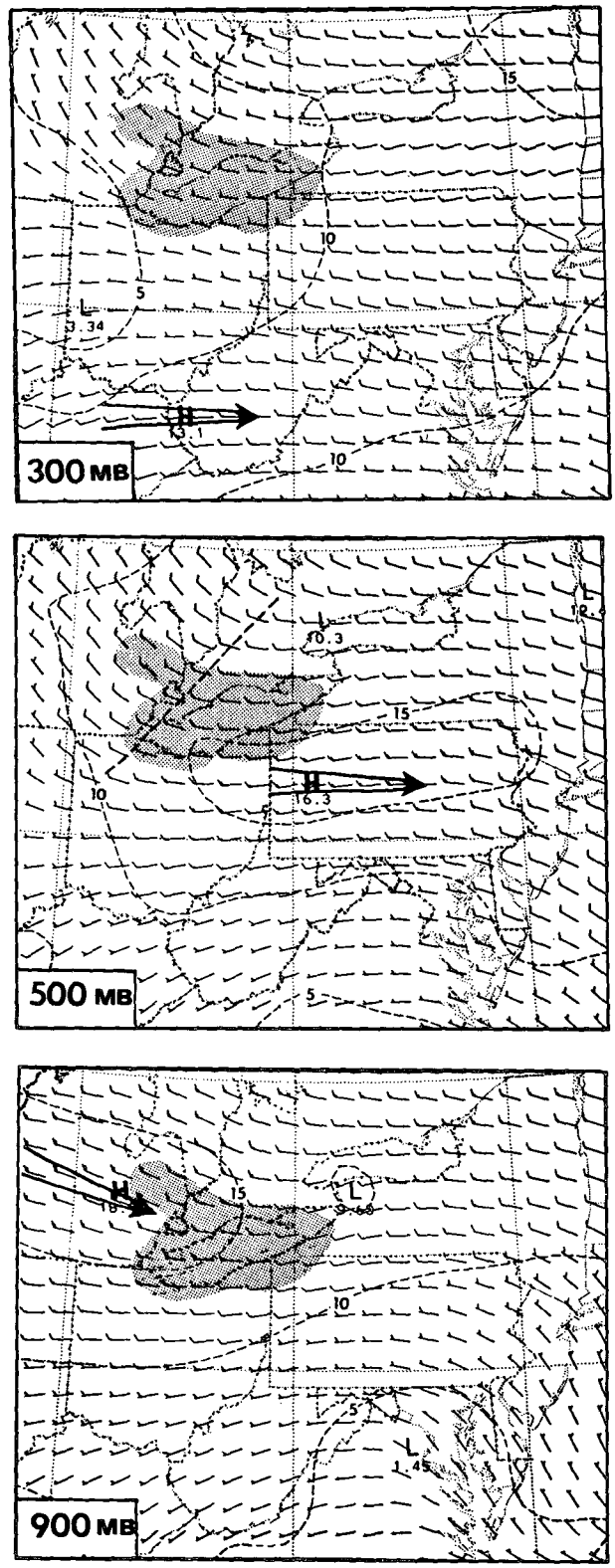

FIG. 2. Mesoscale wind field plotted at every other grid point for 1200 UTC 19 July 1977. Dashed lines denote isotach (full barb = 10 m s^{-1}); large arrows indicate axes of maximum wind speed. Shading denotes the model-predicted area of active convection. Heavy dashed line denotes axis of short-wave trough. "V" indicates location of vortex center.

ellite imagery, this area agrees well with the observed deep cloud coverage at this time (see Fig. 10 in ZF86). At 500 mb, anticyclonic flow dominates the extreme western portion of the domain, and indicates the approach of a large-scale ridge. On the other hand, in the central and northeastern portions of the domain, cyclonic flow associated with a short (meso-α scale) wave prevails. At 900 mb, there is a westerly jet intersecting the MCS over eastern Michigan and Lake Erie. As found by Maddox (1983) and Merritt and Fritsch (1984), the appearance of a low-level jet is a common feature associated with most MCCs. Note that the low-level westerly jet is overlain by relatively weak flow at middle and upper levels, and there is no well-defined upper-level jet axis. Farther to the east and southeast of the MCS, upper-level winds are stronger. Kinematically, this implies that low-level convergence and upper-level divergence are present in the vicinity of Lake Erie and northwestern Pennsylvania. Note also the relatively weak horizontal deformation over most of the domain that, as discussed later, provided a favorable environment for the development of the mesovortex.

Six hours later (1800 UTC), a significant wind perturbation developed at all levels as rapid generation of the mesovortex ensued over northwestern Pennsylvania (see Fig. 3). Low-level westerly winds were greatly enhanced just to the south of the location where the mesovortex was developing. In particular, for both the 900 and 500 mb levels, note the maximum/minimum wind speed couplet associated with the incipient mesovortex. This couplet extends above 500 mb and becomes a strong divergent anticyclonic flow with intense cross isobaric motion (not shown) around its center at 300 mb. According to Fritsch and Brown (1982), this is a consequence of the rapid change in horizontal height gradient when air parcels ascend vertically through a deep layer in the mesovortex and then diverge horizontally within a very thin layer. The upward motion in this case, as will be seen in the next section, is more than 1 m s^{-1} at 500 mb. At 300 mb, the mesoanticyclone behaves like an "obstacle" embedded in the westerly flow. It slows down approaching air parcels and then forces them to divert. Wetzel et al. (1983), Fritsch and Maddox (1981), and Maddox et al. (1981) found similar features at 200 mb for the MCCs they studied.

By 0000 UTC, the influence of the mesovortex and deep convection on the mesoscale flow had expanded as the mesolow deepened and the MCC intensified (see Fig. 4, and ZF86). The low-level westerly jet upstream of the MCC shifted southward in association with the southeasterly propagation of the short wave, the mesovortex and the MCC. Low-level meso-β scale flow around the mesovortex strengthened and exhibited a closed cyclonic circulation with strong cross-isobaric motion toward its center. Interestingly, the 500 mb flow around the vortex weakened slightly; however, it exhibited a considerably larger area of influence. This

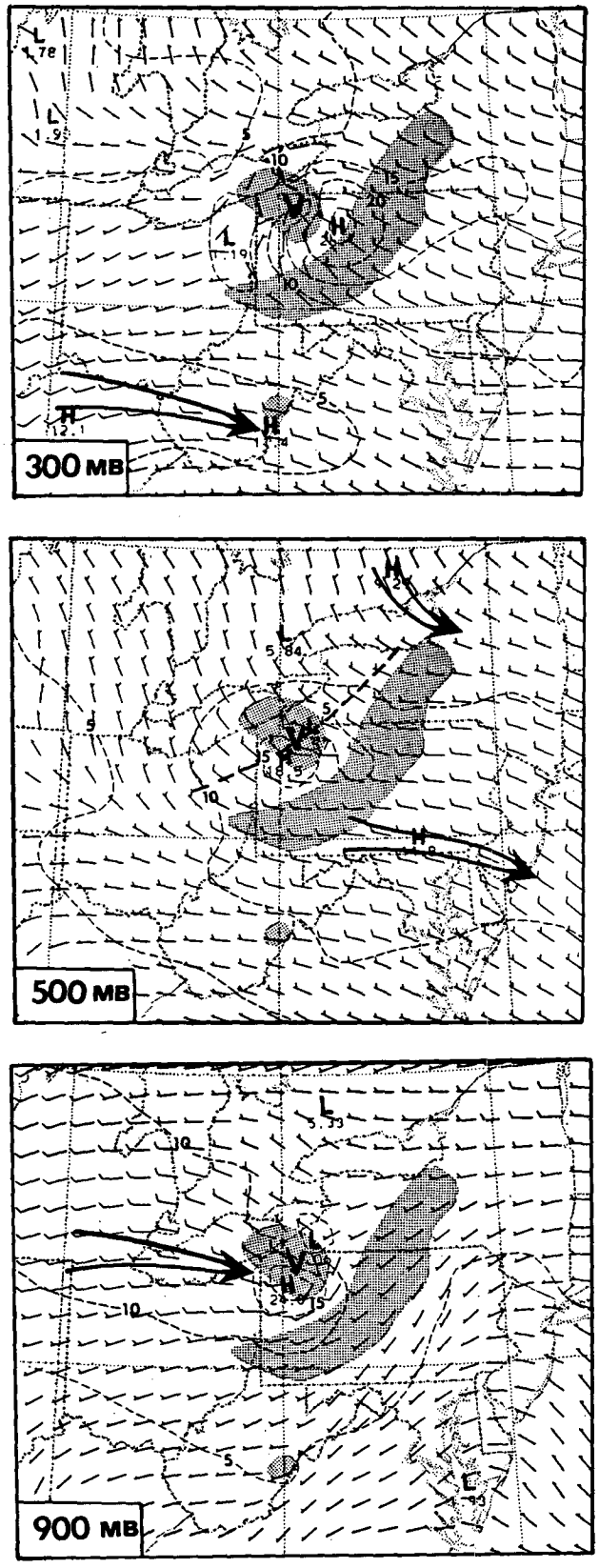

FIG. 3. As in Fig. 2 except for 6-h forecast verifying at 1800 UTC 19 July 1977.

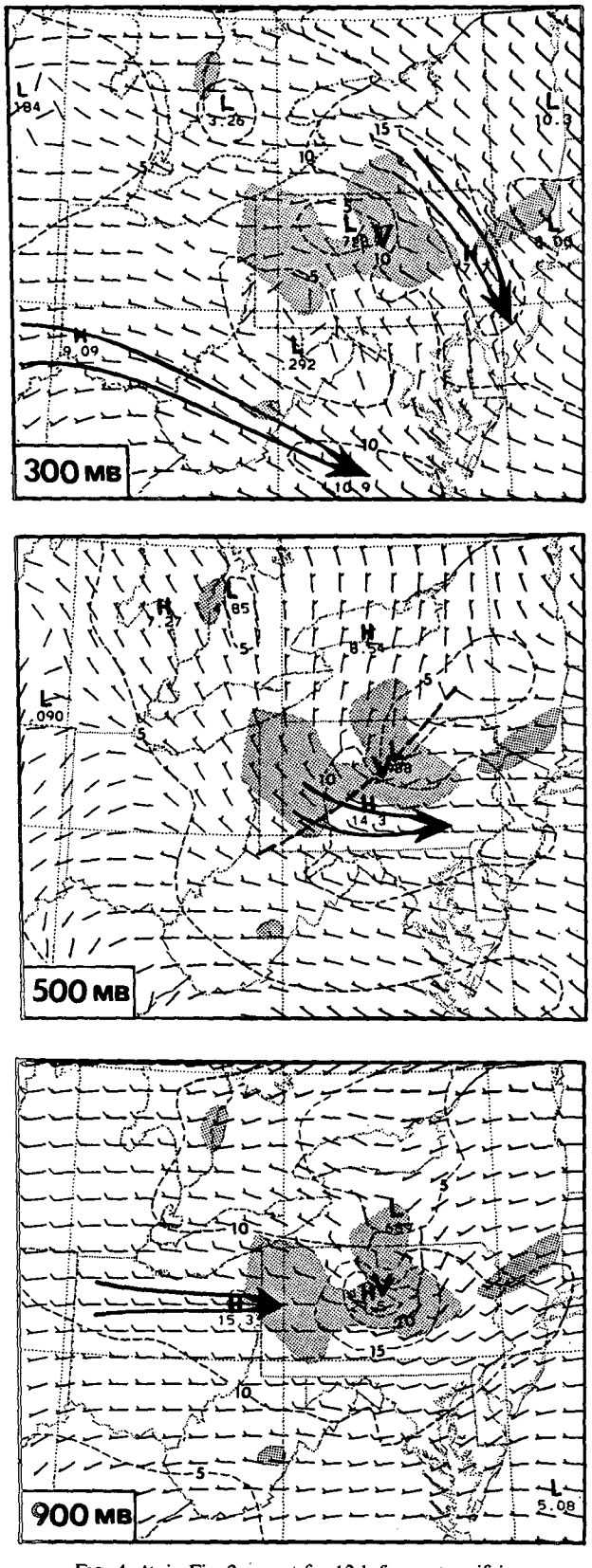

FIG. 4. As in Fig. 2 except for 12-h forecast verifying at 0000 UTC 20 July 1977.

agrees with the results of Maddox (1983) who noted that the changes in the environmental flow tended to be the smallest at midlevels. On the other hand, the changes at 300 mb were quite dramatic. The cyclonically curving westerly winds over the northeastern quadrant were replaced by a broad anticyclonic flow. Moreover, a northwesterly jet developed northeast of the mesovortex in the same relative location as the "convectively driven" jet streaks found by Fritsch and Maddox (1981). Note also that the "obstacle" effect of the MCC expanded into two weak wind zones, apparently in response to the two main areas of deep convection and the mesovortex.

During the evening hours (see Fig. 5), the persistent low-level jet continuously supported deep convection along the western Pennsylvania border; however, the convection was not as well organized as a few hours earlier, i.e., the convective area diminished (see Fig. 6 and ZF86). The same jet also produced mass convergence over northern Maryland and helped initiate new convection along the southeastern periphery of the convective system. The maximum wind associated with the mesovortex diminished and the cyclonic circulation weakened as the surface mesolow broadened and filled (see Figs. 5 and 6). At 500 mb, anticyclonic flow now dominated almost the entire western half of the fine-mesh domain, indicating the continued eastward advancement of the large-scale ridge. Meanwhile, the axis of the short-wave trough rotated to a NE–SW orientation, as the southern portion of the wave slowed its eastward movement and shifted to a more southerly direction of propagation. While this adjustment in the direction of propagation of the southern portion of the short wave may be entirely the result of upper-level quasi-geostrophic processes, it may also be a reflection of the fact that vortices of this scale tend to propagate to the right of the mean flow (see Chan, 1984). In this regard, note that the 900 and 500 mb circulation centers are nearly coincident and that the scales are now much more comparable than in the early stages of the mesovortex.

The dramatic changes that occurred previously in the 300 mb winds (see Figs. 3 and 4) are less apparent at this time (cf. Figs. 3, 4 and 5). Instead, the major wind adjustments are now more prominent at approximately the 200 mb level (see Fig. 5) and are even larger than those noted at 0000 UTC. Specifically, the jet streak that appeared northeast of the convective complex at 0000 UTC is now much more well developed and clearly fits the characteristic pattern that is commonly observed with mesoscale convective complexes. Note that in response to the persistent convection over western Pennsylvania, a new "streak" has appeared over north central Pennsylvania so that two couplets of high and low winds are readily apparent. Note also that now the entire domain is dominated by anticyclonic flow.

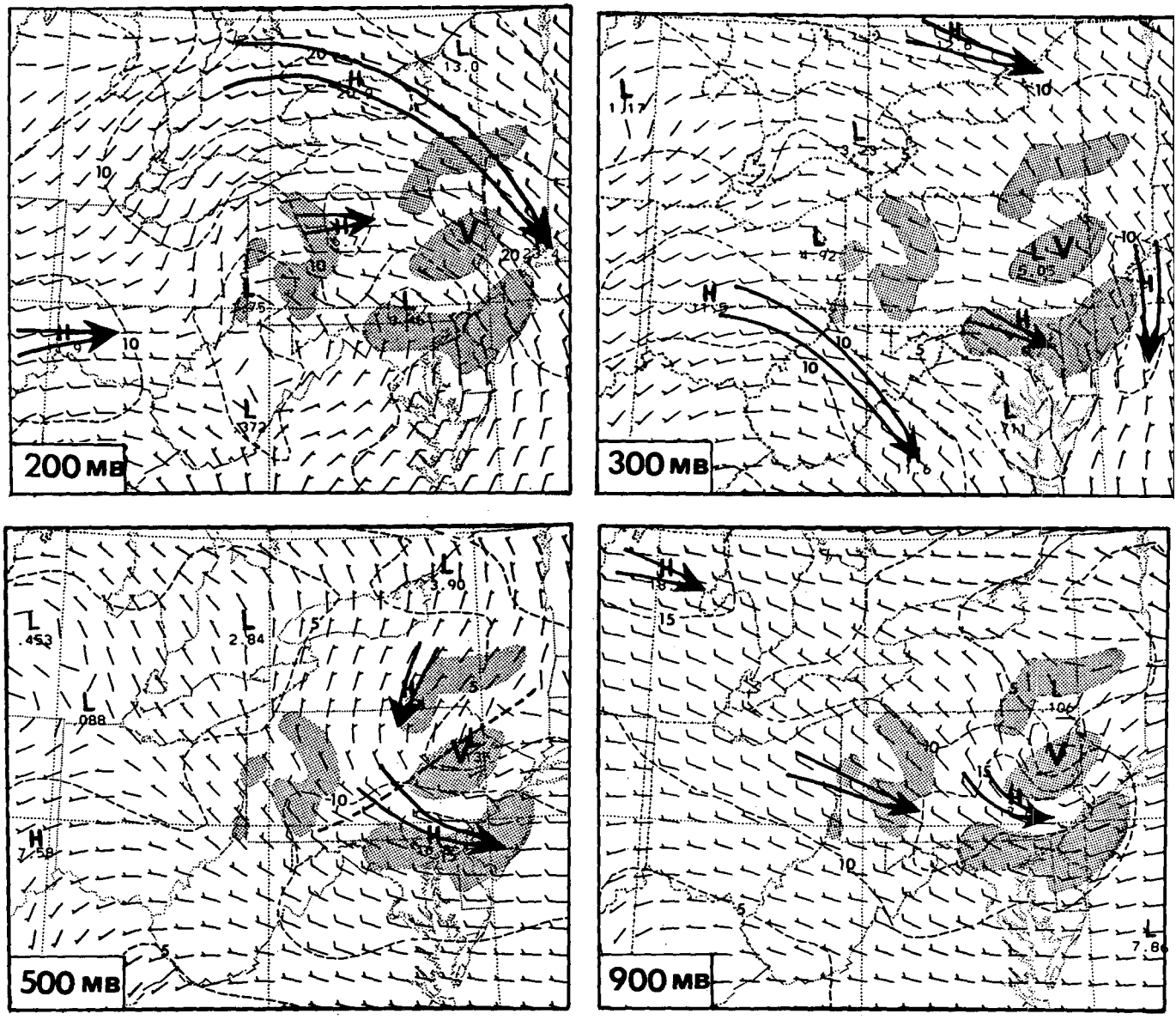

FIG. 5. As in Fig. 2 except for 18-h forecast verifying at 0600 UTC 20 July 1977 and including 200 mb winds.

3. Evolution of vertical structure and midtropospheric warm core

Figure 6 shows the locations of various cross sections relative to surface pressure perturbations, areas of active convection, and outflow boundaries at 1800, 0000 and 0600 UTC. The locations were selected to display the thermodynamic and kinematic structure of the most significant mesoscale features. The vertical cross sections of the predicted potential temperature (θ), relative humidity, divergence, vertical motion, equivalent potential temperature (θ_e), vorticity and horizontal wind fields at 1800 UTC are shown in Fig. 7. As the surface mesolow deepened during the initial six hours of the simulation, tremendous intensification of vertical motion and concentration of vorticity occurred. Figures 7a and 7b show strong low-level convergence and upper-level divergence with an intense vertical circulation. Upward motion more than 1 m s^{-1} developed at 500 mb and vorticity values became as large as 10^{-3} s^{-1} (Fig. 7d). No indications of such large values of vorticity were present in the initial conditions (not shown). Thus, such midlevel vortex spinup and its surface counterpart apparently were energetically forced by strong physical processes, such as latent heating. This is discussed further in the next two sections. The strong tangential wind is a consequence of a rapid adjustment of the wind field toward the mass field through the thermal wind relationship. One of the most important characteristics of the mesovortex is that it exhibits a mid-

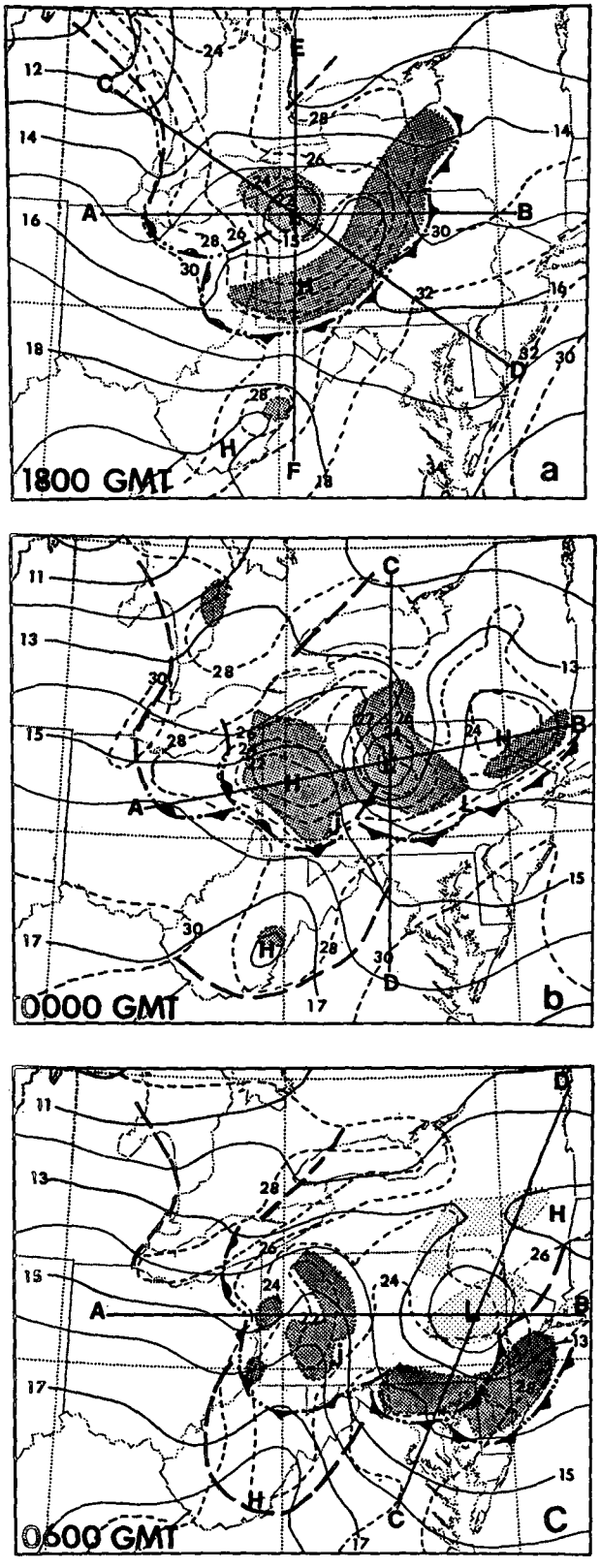

FIG. 6. Analysis of sea level pressure (solid lines, mb) and surface temperature (dashed lines, °C) for (a) 6-h, (b) 12-h, (c) 18-h forecasts. Lines labeled A–B, C–D and E–F indicate location of cross sections shown in subsequent figures. Shaded area indicates location of simulated deep convection. Lighter shading in (c) indicates relatively shallow moist convection.

tropospheric "warm core." Beneath the warm core, a cool pool extends from the surface up to roughly 850 mb. Above the warm core, a cold dome develops between 200 and 300 mb (see Figs. 7a, b and c). The warm core apparently results from the surplus of latent heat release over the adiabatic cooling and the horizontal energy dispersion. In particular, note that the equivalent potential temperature and the horizontal momentum are nearly uniformly distributed within the vortex layer. The vertical uniformity of horizontal momentum has been observed by Ogura and Liou (1980) and Smull and Houze (1985) in an MCS with a trailing region of stratiform precipitation, and also by Zipser et al. (1981) in a slowly moving tropical convective band. It is likely that the vertical uniformity of horizontal momentum provides an important moisture and energy- (especially heat) preserving mechanism for the rapid generation and maintenance of the warm-core structure. Specifically, the small vertical wind shear and weak horizontal deformation slow down the transport of moisture and energy away from the region of mean moist ascent (see Gray, 1968, 1979; McBride and Zehr, 1981; Tuleya and Kurihara, 1981) and this in turn enhances the hydrostatic pressure falls responsible, in part, for the rapid spinup of the mesovortex. Furthermore, based on nonlinear inertial stability arguments, the strong cyclonic rotation of horizontal winds in a deep layer tends to generate resistance to radial displacement of air parcels, and helps to maintain the warm core structure (see Ooyama, 1982; Schubert and Hack, 1982). Note also a nearly moist adiabatic and saturated thermodynamic stratification between 850 and 250 mb in the vortex layer; lower θ_e air is present below this layer (see Fig. 8).

Throughout much of the troposphere, wind flows accelerated as they approached the developing vortex and rapidly decelerated after passing the center/axis of the vertical system (Figs. 7c and 7d), basically satisfying the principle of angular momentum conservation. In the upper troposphere ($\approx$300 mb), a strong outflow appeared downstream of the vortex and an "obstacle" effect (almost vanishing wind speed) developed upstream. This is a consequence of potential/kinetic energy conversion, namely, the upper-level mesohigh resulting from vertical circulations tends to block incoming horizontal flow while accelerating outgoing flow. The vertical structure of the developing mesovortex can be better visualized from a cross section of relative vorticity. Figure 7d shows the incipient vortex pattern with low-level cyclonic circulation and upper-level anticyclonic flow. This feature agrees well with Bosart and Sanders' (1981) diagnostic computations, but the model-produced vorticity values are larger

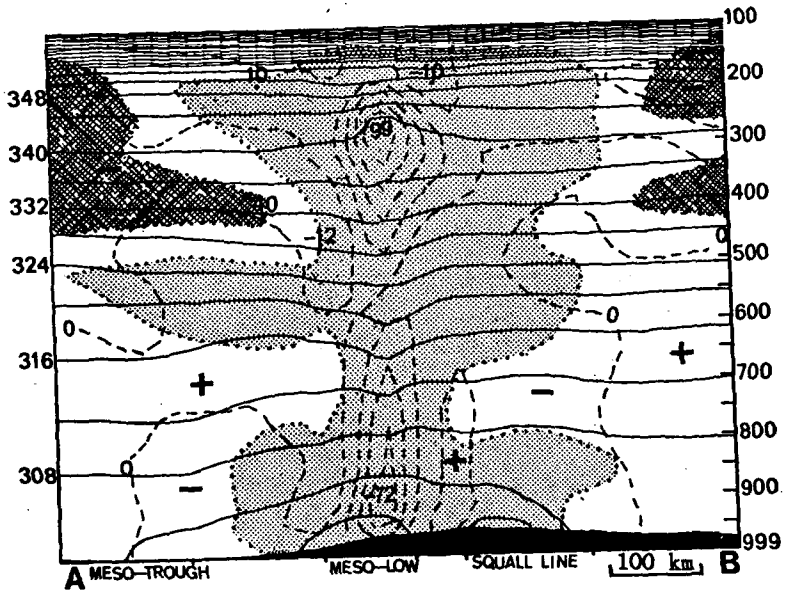

FIG. 7a. Vertical cross section of potential temperature (solid lines, K), divergence (dashed lines, contour interval 20×10^{-5} s^{-1}) and relative humidity (shaded area is $\geq$80% and cross-hatched area $\leq$40%). The section is taken along line AB in the 6-h forecast (see Fig. 6a). Large $\pm$ signs indicate the sign of the divergence in regions where the divergence is small.

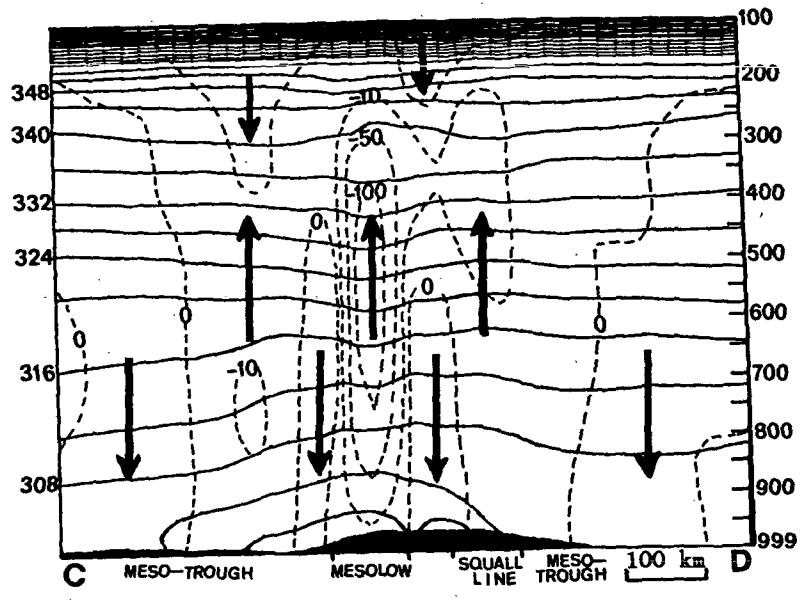

FIG. 7b. Vertical cross section of potential temperature (solid lines, K) and ω (dashed lines, μb s^{-1}). The section is taken along CD in the 6-h forecast (see Fig. 6a). Large arrows indicate direction of vertical motion.

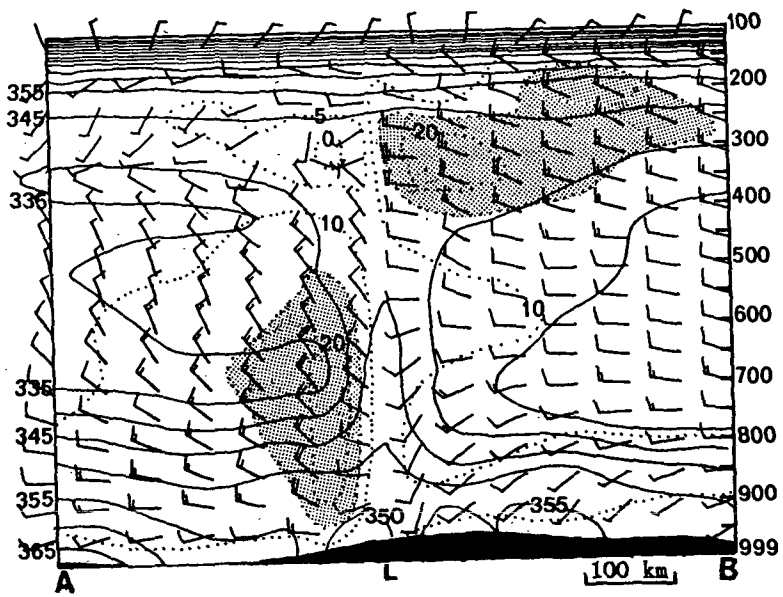

FIG. 7c. Vertical cross section of horizontal winds (speed, m s^{-1}; direction, common convention) and equivalent potential temperature (solid lines, K). The section is taken [illegible] the 6-h forecast (see Fig. 6a). Dotted lines are isotachs with speeds

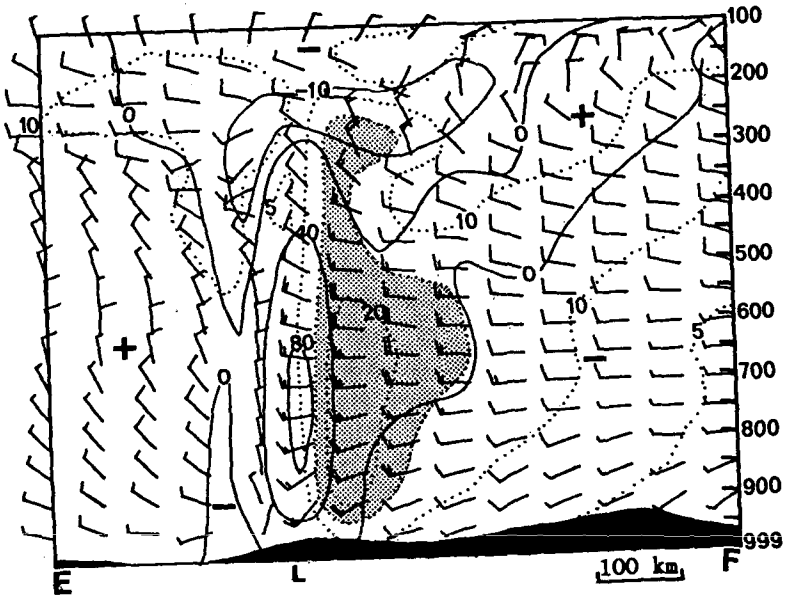

FIG. 7d. Vertical cross section of horizontal wind (speed, m s^{-1}; direction; common convention) and relative vorticity (solid lines, 10^{-5} s^{-1}). The section is taken along line EF in the 6-h forecast (see Fig. 6a). Dotted lines are isotachs (m s^{-1}) with speeds $\geq$15

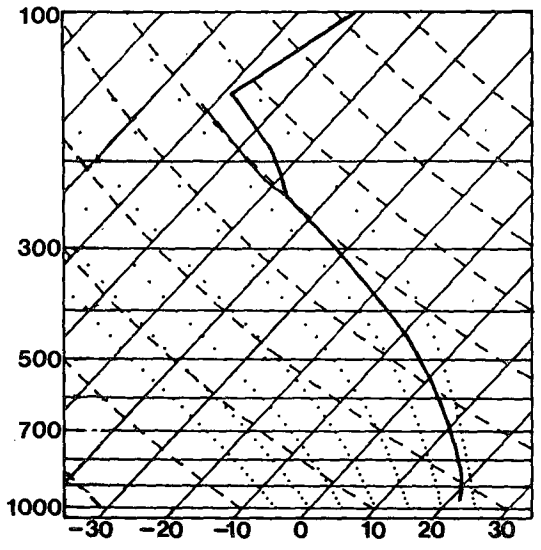

FIG. 8. Skew T–log P plot of a sounding taken near the center of the mesolow from the 6-h forecast.

(possibly due to the different grid resolution or an overprediction of the mesolow). Likewise, when compared to another vortex event (Menard et al., 1986), the model-produced vertical distribution of vorticity is similar, however, the model-generated magnitudes are again larger than that diagnosed from the data. Note though that the model can resolve smaller scales (and therefore greater magnitudes) than can be resolved by the standard upper-air observing network.

As shown in ZF86, there is initially only one area of convection. This area split later into a squall line and a trailing convective region that eventually became the MCC responsible for the Johnstown flood. One possible explanation for the separation of the squall line from the pre-MCC is apparent from Figs. 7a and 7b. Specifically, as the mesovortex becomes well developed, the strong descending branch of the vertical circulation suppresses convective development between the pre-MCC and the squall line, and thereby splits the two areas of deep convective activity. This argument can possibly be used to help explain the separation of a squall line from a midlevel vortex in the case studied by Smull and Houze (1985). Note, however, that the model convection over Lake Erie (Fig. 6a) continued at this time even though some of it was in the sinking branch of the vortex circulation (see Fig. 7b). This can be explained by the assumption implicitly included in the Fritsch–Chappell convective parameterization scheme that convective effects, once initiated within an environment with available buoyant energy and upward motion, will last for the entire convective time period, τ_c, no matter how the larger-scale environment behaves during the period (see Fritsch and Chappell, 1980; and ZF86). An alternate explanation for the splitting is based upon internal gravity wave arguments. In particular, such waves may be instrumental in initiating deep convection (see Uccellini, 1975; Eom, 1975; Miller and Sanders, 1980) so that a line of thunderstorms could advance away from the initial convective source region faster than the traveling meso-α scale forcing features that were responsible for the initial convection (see ZF86). Thus, the more slowly evolving meso-α scale feature could conceivably force the development of additional deep convection in the same general region where the initial convection occurred. This combination of events would give the appearance of a "splitting" system. A more detailed presentation of the splitting and its association with gravity waves will appear in a forthcoming article.

Cross sections for the 12-h forecast (Fig. 9) show that the mesovortex continued to spin up during the 6 hours from 1800 to 0000 UTC and that a closed cyclonic circulation is clearly apparent through most of the troposphere (see Fig. 9c). However, the cross section of vertical motion indicates that upward motion in the warm-core vortex has weakened (cf. Figs. 7b and 9a). Note that the supply of high-θ_e air to the vortex is now being intercepted by deep convection over western Pennsylvania (see Figs. 4, 6 and 9b), and low-θ_e air from midlevels is entering the vortex's circulation. These factors suggest that the vortex is about to "spin down." Note also that the vertical motion associated with the squall line decreased as the squall line moved eastward and weakened.

If it is assumed that cloudy regions are approximated by the $\geq$80% relative humidity areas, then the shading in Figs. 7a, 9a and 10a shows extensive regions of low, middle and upper level clouds. In particular, note the "anvil" cloud covering virtually the entire length of Pennsylvania. This compares reasonably well with the enhanced infrared satellite image for those times (see Fig. 10 in ZF86). It is also apparent in Figs. 7a, 9a and 10a that dry air at middle and upper levels is intruding into the western portion of the domain. This is consistent with the analysis of Hoxit et al. (1978). The presence of the moist downdraft air in the boundary layer is clearly visible in the west–east cross section of equivalent potential temperature, i.e., there is a strong θ_e inversion below 900 mb and conditionally unstable conditions above on either side of the vortex. This structure conforms to the Pittsburgh θ_e profile at 0000 UTC (see Fig. 7 in Hoxit et al., 1978). Within the mesovortex, the θ_e inversion in the lowest layer, the θ_e minimum in the middle troposphere and the undilute ascent above the planetary boundary layer (PBL) within the mesovortex are all similar to the observed structure of a hurricane rainband analyzed by Barnes et al. (1983) and a tropical convective system studied by Zipser et al. (1981). It is also apparent from Figs. 9a and b that the moist air entering the MCC comes from the upper portion of the mixed layer that developed to the west of Pennsylvania. This air is forced to rise as it overruns the shallow pool of cool moist downdraft air from previous deep convection.

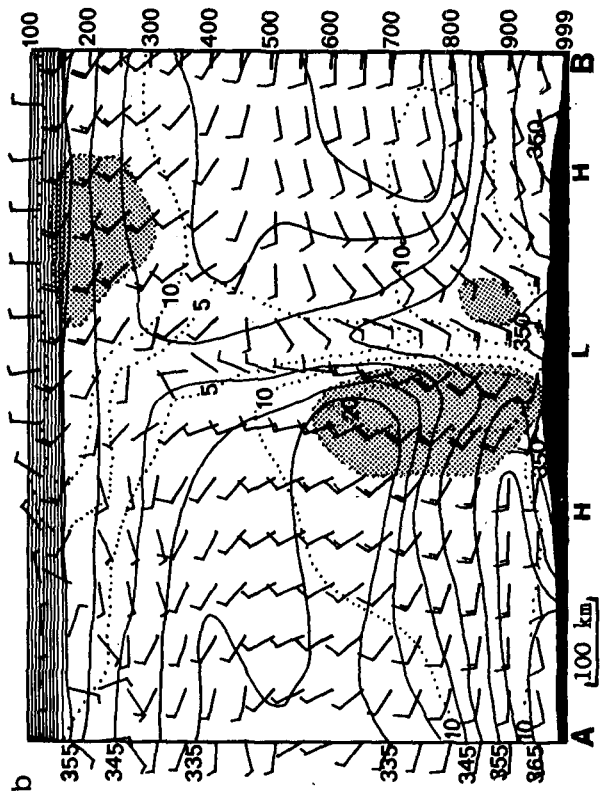

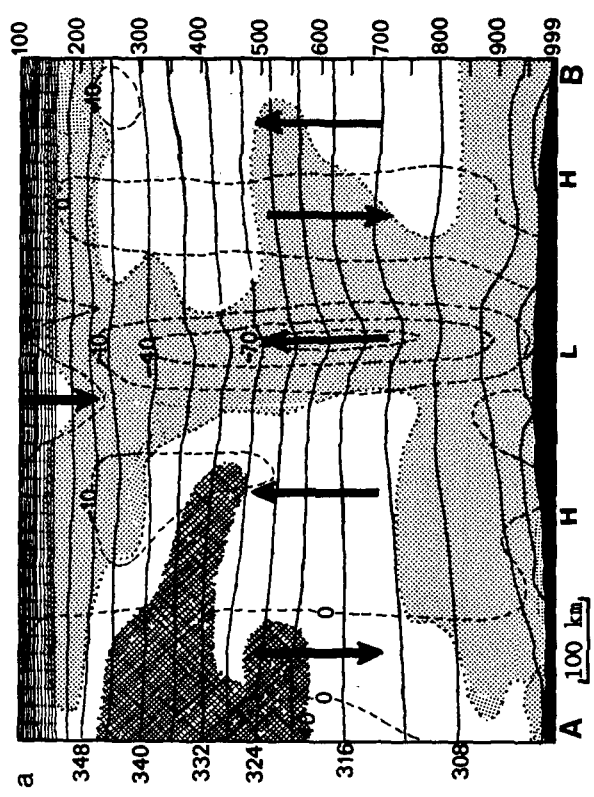

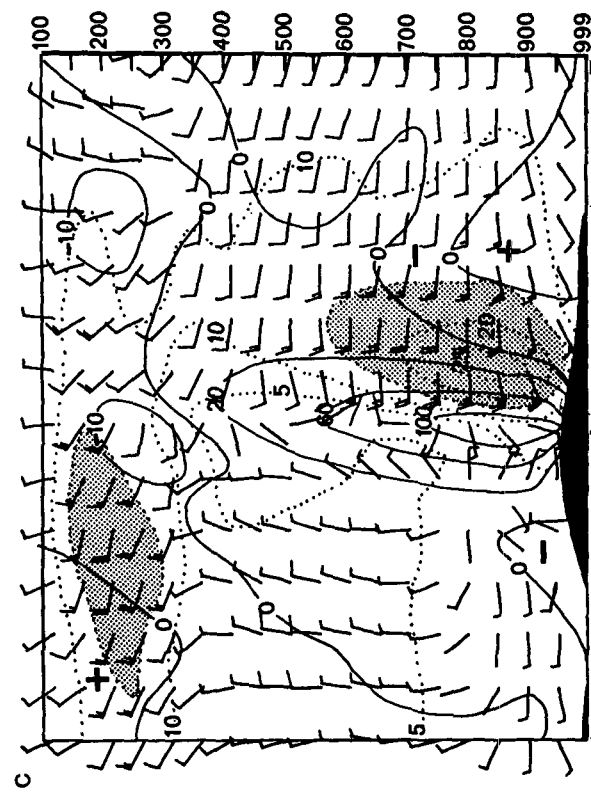

FIG. 9. (a) Vertical cross section of potential temperature (solid lines, K), ω (dashed lines, $\mu b\ s^{-1}$) and relative humidity (shaded area is $\geqslant 80\%$ and cross-hatched area $\leqslant 40\%$). The section is taken along line AB in the 12-h forecast (see Fig. 6b). (b) As in Fig. 7c except for the 12-h forecast along line AB (Fig. 6b). (c) As in Fig. 7d except for the 12-h forecast along line CD (Fig. 6b).

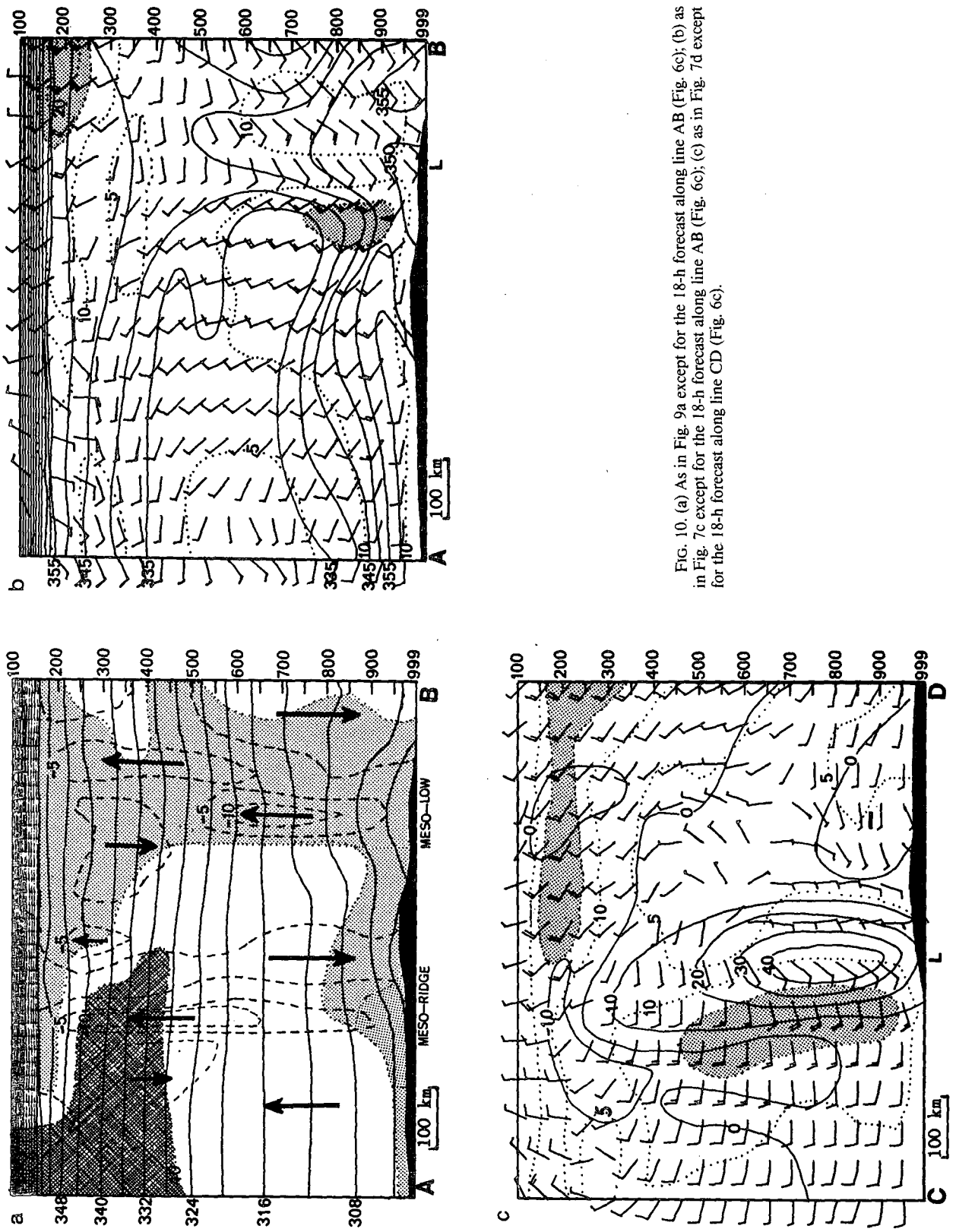

FIG. 10. (a) As in Fig. 9a except for the 18-h forecast along line AB (Fig. 6c); (b) as in Fig. 7c except for the 18-h forecast along line AB (Fig. 6c); (c) as in Fig. 7d except for the 18-h forecast along line CD (Fig. 6c).

Figure 10 shows cross sections of the 18-h forecast (verifying at 0600 UTC 20 July) along lines AB and CD in Fig. 6c. The mesovortex, as indicated before, has "spun down" and now exhibits a smaller temperature excess and much weaker and shallower upward motion than six hours ago. Also, the low-level cool pool is deeper and stronger than earlier, and the vortex tilts slightly with height (Fig. 10c). However, the relative humidity and equivalent potential temperature change very little within the vortex column (Figs. 10a and 10b). As discussed in section 5, the braking effect by convection (particularly moist downdrafts) resulted in the "spin down" of the vortex while the inertial stability of the rotational winds and weak deformation contributed to the maintenance of the vertical uniformity of the vortex properties. While the mesovortex has rapidly spun down, the central pressure of the surface mesolow increased by only one millibar during the last six hours (see Figs. 6b and 6c). Note also that the mesolow has broadened considerably, i.e., the radius of the 1012 mb isobar with the mesolow has significantly increased. This broadening of the mesolow also appeared to occur in the analysis of Hoxit et al. (1978) and ZF86. To the west of the mesovortex and MCC, horizontal winds exhibit only slight veering with height, implying much weaker warm advection compared to six hours ago. Of particular interest is the vertical circulation, comparable in strength to that of the mesovortex, that has developed over western Pennsylvania. This feature is consistent with the observed continuation of deep convective activity and trough development over that region (see ZF86). Notice, however, that the maximum mesoscale vertical motion associated with the deep convection is near the 400 mb level while the maximum associated with the mesovortex is around 600 mb. This difference reflects the tendency for convective heating from intense thunderstorms to be shifted to relatively high levels by the eddy flux terms (Anthes, 1977) while for the resolvable-scale latent heat release, no such vertical shift is possible and the maximum heating tends to be at lower levels. Consequently, deep convection tends to enhance midlevel convergence while resolvable-scale heating is more likely to increase low-level convergence (see Fritsch, 1986; Levy and Cotton, 1984). It is interesting to note that a recent diagnostic study of a larger-scale tropical system (Johnson, 1984) indicates the opposite. This disagreement may be a result of many things, e.g., the scale of the system, differences in the large-scale environment, the type of convective system and the methodology of the diagnostic study. In fact, in a detailed diagnostic study of a severe midlatitude convective system that occurred during SESAME, Kuo and Anthes (1984) found that the level of maximum heating gradually *lowered* as the system matured. Note that midlatitude convective systems are often characterized by very deep and intense convection at the beginning of the system and by more mesoscale circulations as the system matures (Maddox, 1980, 1983). On the other hand, tropical systems exhibit their deepest and strongest convection much later in the lifetime of the system (Frank, 1978).

A natural question here is why the deep convection over western Pennsylvania persisted within an environment where the lowest layers (below 900 mb) were convectively stable and there was little warm advection higher up. A possible interpretation is as follows. The edge of the cool pool of moist downdraft air from previous convective storms behaves as a quasi-stationary warm front with a slant surface wedged into the convectively unstable air to the west. Thus, westerly winds are forced to ascend over this slantwise surface. Air embedded in such anabatic flow ascends the sloping surface and releases the potential buoyant energy. This mechanism can be visualized from Figs. 10a and 10b in which slantwise θ_e-surfaces, the low-level jet, and weak ascending motion up to the midtroposphere are juxtaposed. The location of active convection corresponds to the high "plateau" following the constant θ_e surfaces (see Fig. 10b). It is also possible that terrain may be playing a significant role in increasing the slope of the θ_e-surfaces. In a sensitivity experiment, Zhang (1985) showed that with a smoothed terrain as the lowest model boundary, the model fails to reproduce the continued evening convection over western Pennsylvania.

Finally, it is helpful to compare the model-generated thermal structure of the mesovortex to a preliminary analysis of a Pre-STORM MCC-generated vortex. Figure 11 shows the evolution of the model-generated 500 mb temperature distribution. The well-developed vortex exhibits 2°–3°C warming compared with its ambience. Although it is almost impossible to verify from observations on this fine scale, the Hoxit et al. analysis shows a midlevel warming ≥ 2°C on a much broader scale (see Figs. 7 and 24 in ZF86). Very encouragingly, the temperature analysis of the Pre-STORM event agrees with the model-generated structure and magnitude of the warm-core features. Figure 12 displays the 500 mb wind and temperature analyses for this event. A strong cyclonic circulation with a 2°–3°C warm-core temperature perturbation is clearly apparent (see Johnson, 1986 for a detailed description of the case).

4. Grid-resolvable scale precipitation

Zhang and Fritsch (1986a) have shown that the model-predicted distribution and magnitude of 12-h accumulated total rainfall conform fairly well to the analyses of Hoxit et al. (1978) and Bosart and Sanders (1981). Figure 13 shows the horizontal distribution of the predicted 12-h and 18-h accumulated grid-resolvable scale precipitation. The axis of the heaviest rainfall correlates well to the path of the mesovortex (see Fig. 1c) and the transverse dimension roughly reflects the

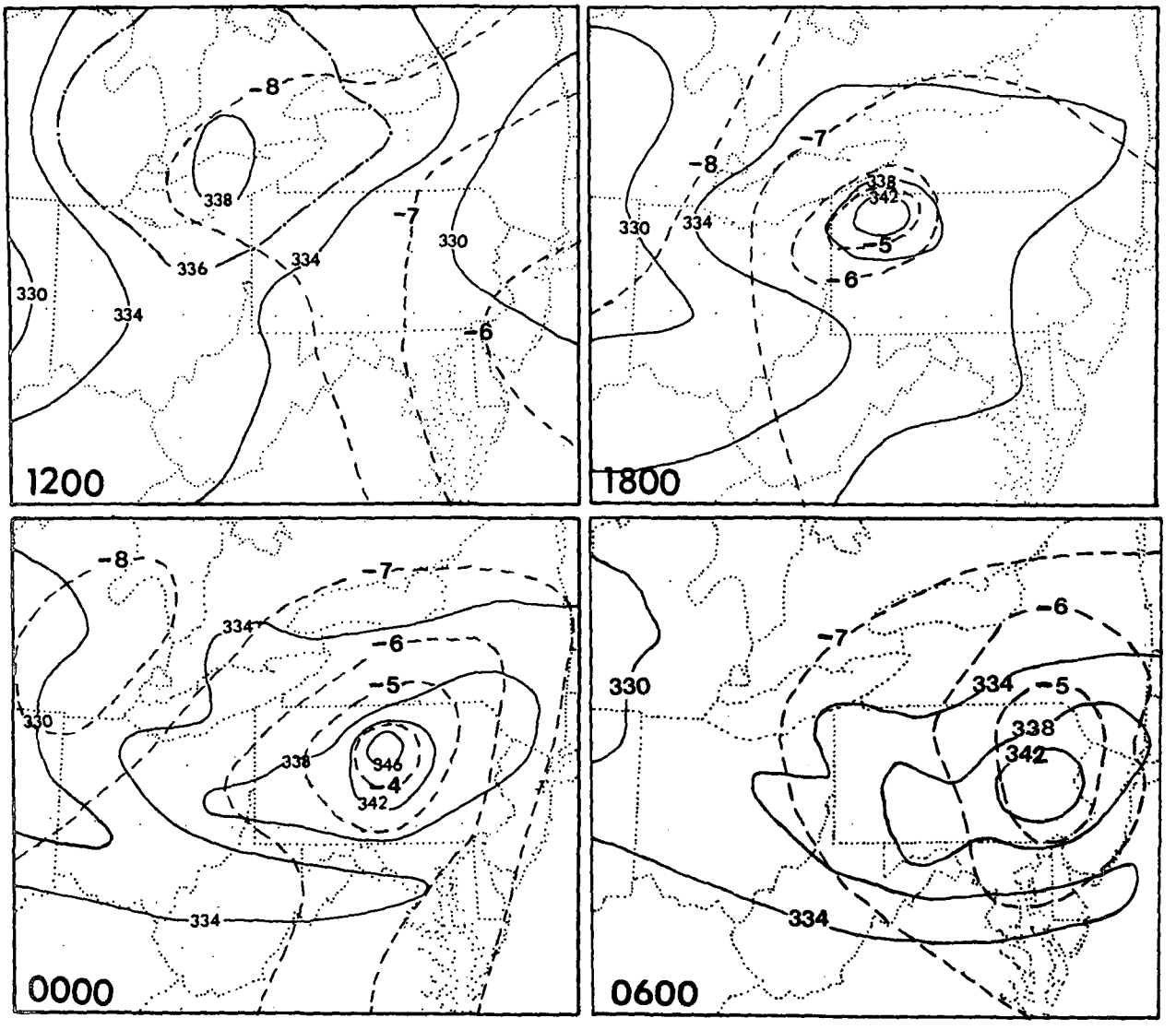

FIG. 11. Predicted evolution of 500 mb equivalent potential temperature (solid lines, K) and temperature (dashed lines, °C).

size of the mesovortex. It is interesting to note that during evening hours (from 12 to 18 model hours), a sizeable area of resolvable-scale precipitation developed just to the west of Johnstown, Pennsylvania. This coincidentally corresponds to the location of the observed flooding event (see Hoxit et al., 1978), and in the model it resulted from mesoscale convergence forced by persistent (≥8 h) convective development over western Pennsylvania. Hourly analyses of resolvable-scale precipitation (not shown) indicate that the rainfall maximum in northwestern Pennsylvania was primarily generated during the first nine hours of the simulation. The observed rainfall over this region is around 12–25 mm h^{-1} for at least six hours (see Hoxit et al., 1978). Furthermore, the time evolution of accumulated precipitation shows that the model produced more resolvable-scale than convective precipitation during the fifth to the ninth hours as the mesovortex intensified (see Fig. 14). The model prediction of resolvable-scale rainfall over northwestern Pennsylvania during this time period is also supported by radar analyses. For example, Fig. 15 shows a tracing of the Pittsburgh radar scope at 1735 UTC 19 July. Notice the large region of level 1 and 2 returns over northwestern Pennsylvania. The squall line, with level 3 and 4 returns, is clearly evident over central Pennsylvania. After the 12th model hour, only a small amount of resolvable-scale precipitation occurred. This agrees with the weakening of the mesovortex. On the other hand, accumulated convective rainfall increased linearly, and this corresponds to the continuation of deep convection over western and southern Pennsylvania.

In a dual-MCC case study, Rockwood et al. (1984) also recognized the importance of the development of

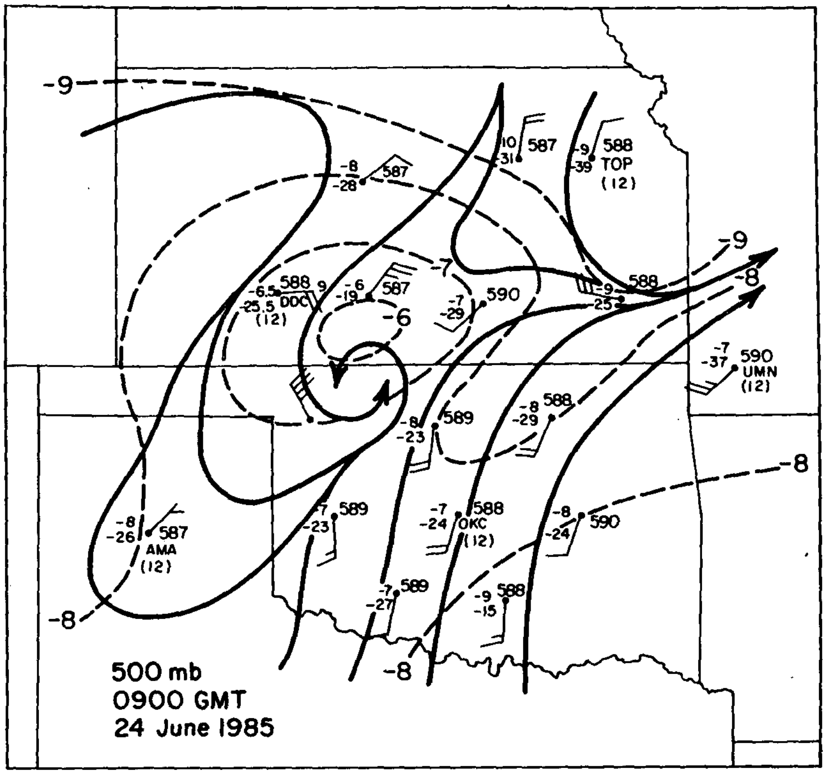

FIG. 12. Analysis of 500 mb streamlines (solid lines) and isotherms (dashed lines, °C) for a Pre-STORM mesovortex (reproduced from Johnson, 1986).

the mesolow in association with the stratiform precipitation pattern. Moreover, in a radar and satellite observational study, Smull and Houze (1985) found a similar correlation of stratiform rainfall with the development of a vortex embedded in an MCC. And in yet another case study, Houze (1977) and Cheng and Houze (1979) calculated that the stratiform component of the precipitation from mesoscale convective systems accounts for about 40% of the total precipitation. These observations support the model-simulated relationship between the vortex and the stratiform (resolvable-scale) precipitation and the fact that the resolvable-scale rainfall accounted for a significant fraction (30%–40%) of the total precipitation in the present simulation (see Fig. 14).

Figure 16 compares the vertical distribution of convective and grid-resolvable scale heating at incipient and mature stages of the mesovortex. Clearly, the resolvable-scale heating far exceeds the heating from the convection. Note though that the resolvable-scale heating is the maximum at a particular grid point at a particular time. At immediately adjacent points, the magnitude of the resolvable-scale heating is about 50%–70% of that shown in Fig. 16. And at two points away from the maximum, it is only 25%–30%. Because environmental lapse rates are nearly moist adiabatic near the center of the mesolow, the magnitude of the convective heating is much smaller than that at other convectively active portions of the domain (see ZF86). Since the grid-resolvable scale heating occurred in the low to middle troposphere and was much greater than the convective heating, it apparently was energetically responsible for the rapid development of the mesovortex and for the establishment of the warm-core structure.

While the development of the vortex is similar to that which occurs in other theoretical and numerical studies of mesoscale systems (Koss, 1976; Anthes and Keyser, 1979; Anthes et al., 1983; Perkey and Maddox, 1985), the intensity of the vortex in the lowest 100–300 mb of the model seems too large. This overprediction may be the result of gravitational instability (see Kasahara, 1961), i.e., when the atmosphere is saturated with a lapse rate greater than moist adiabatic, small perturbations will grow exponentially with the maximum growth rate at the shortest scale permitted by viscosity (Kuo, 1961). On the other hand, the development of the vortex appears to depend upon the feedback between latent heat release and mesoscale low-level convergence. In this sense it may be more likely a CISK-type instability. For this particular numerical simulation, certain physical processes that slow the low-level developments of such vortices are not included in the model. Specifically, the resolvable-scale conden-

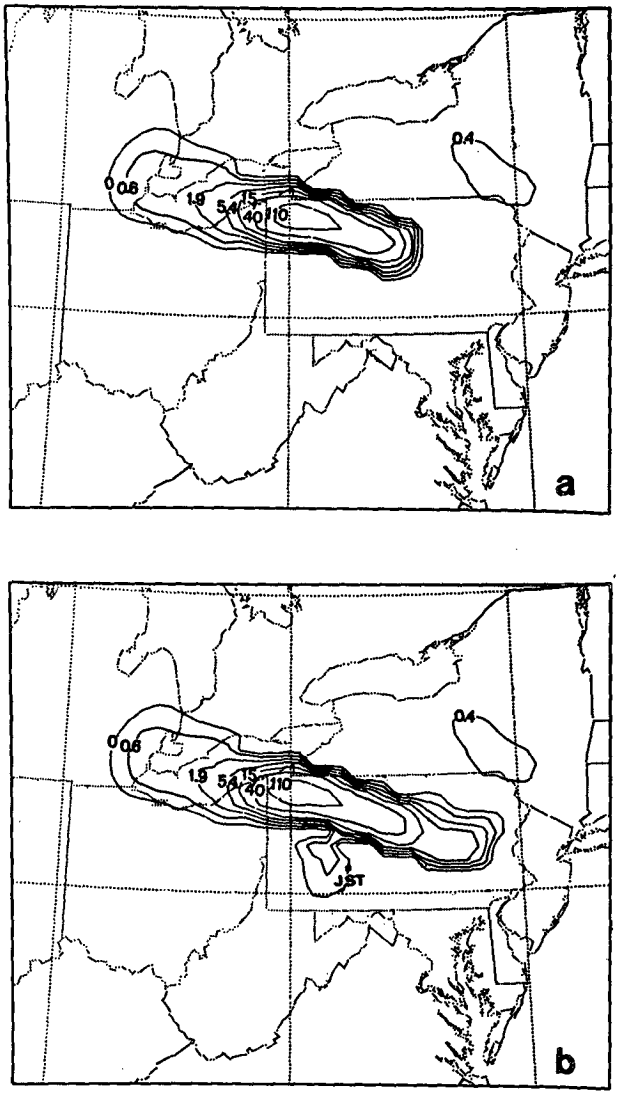

FIG. 13. Predicted accumulated grid-resolvable scale rainfall (mm) for periods (a) 1200 UTC 19 July 1977 to 0000 UTC 20 July 1977 and (b) 1200 UTC 19 July 1977 to 0600 UTC 20 July 1977.

sation was determined simply by removing supersaturation. This method of computing resolvable-scale condensation and its associated heating is almost a standard in *large-scale* models (see Haltiner and Williams, 1980; Kuo and Qian, 1981). However, for fine mesh simulations such as this one, *mesoscale updrafts and downdrafts* are an integral part of the mesoscale convective systems and the condensation/precipitation process (Zipser, 1977; Houze, 1977; Ogura and Chen, 1977; Brown, 1979; Leary, 1980; Maddox, 1983). Although mesoscale updrafts and downdrafts can be described explicitly, accurate simulation of them requires that phase changes occurring on the mesoscale be described realistically. To do this, additional physical processes not usually included in large-scale models should be accounted for. Specifically, resolvable-scale water loading, subcloud layer evaporation and even melting have significant effects on the hydrostatic pressure field and therefore on the mesoscale circulation (e.g., see Zipser, 1977; Brown, 1979; Molinari and Corsetti, 1985; Molinari and Dudek, 1986). These processes tend to stabilize the vertical atmospheric column and slow down the resolvable-scale condensation rate in the low- to midtroposphere. When these processes are included in the simulation of the Johnstown MCCs, it is found that the overprediction of the mesovortex and the central pressure of the surface low are significantly reduced. Detailed description of these results will be published in a future journal article.

5. Discussion

From the results presented in section 4, it is evident that the energy source for the development of the mesovortex and its associated warm-core structure is strongly linked to resolvable-scale condensation. In a numerical model, such condensation usually exhibits a heating maximum at levels relatively lower than that which results from convective cloud heating. Moreover, the sensitivity of the deepening to the lower level of maximum heating is similar to the results from other theoretical and numerical studies (Ooyama, 1969; Anthes and Keyser, 1979; Anthes et al., 1983; Tracton, 1973; Koss, 1976; Sardie and Warner, 1983, 1985; Perkey and Maddox, 1985; Hack and Schubert, 1986). Thus, there appears to be a common process contributing to the rapid cyclonic spinup of several different mesoscale vortices (e.g., polar lows, tropical cyclones, maritime extratropical cyclones, lake vortices, MCC vortices, etc.). This common process is the positive feedback among *low- to midlevel* heating, low-level mass and moisture convergence and surface pressure falls. As mentioned before, the source of the low-level heating in the present case is the resolvable-scale latent

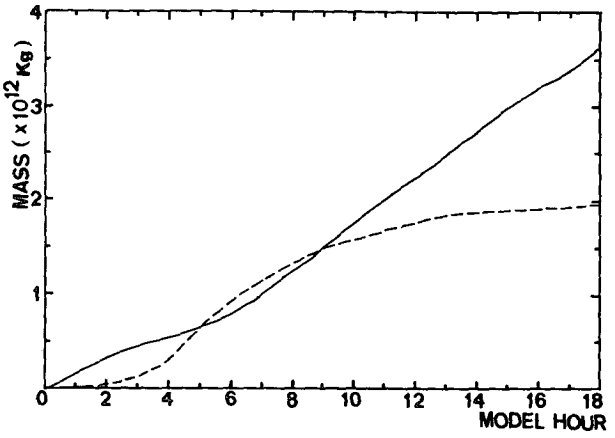

FIG. 14. Time evolution of accumulated rainfall volume (kg) over the fine-mesh domains. Solid and dashed lines indicate convective and grid-resolvable scale rainfall, respectively.

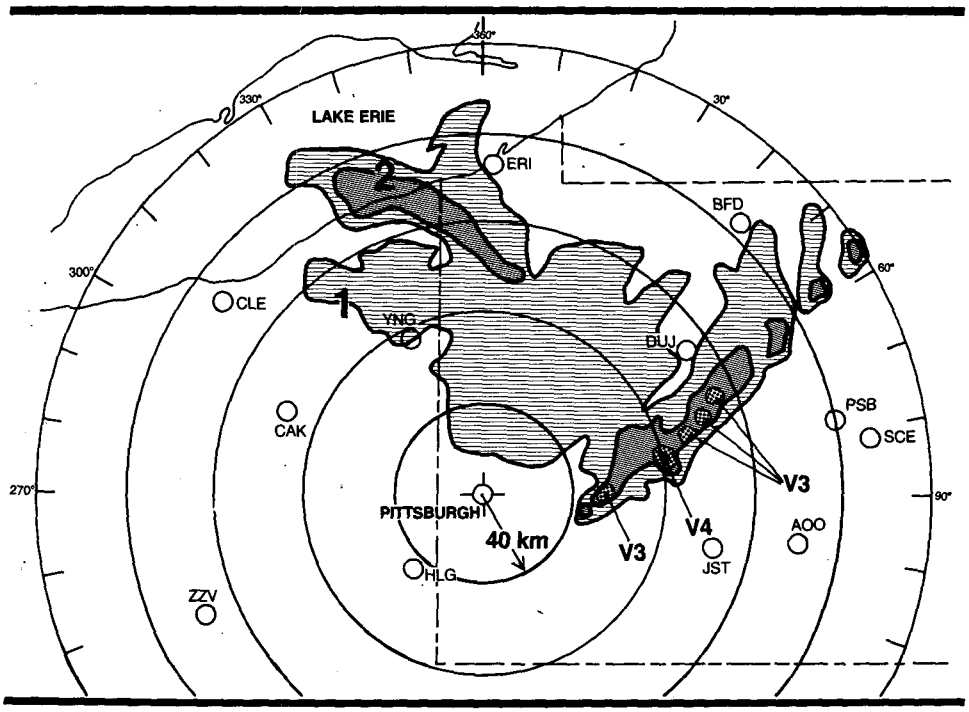

FIG. 15. Tracing of Pittsburgh radar scope at 1745 UTC 19 July 1977. Light and dark shading indicates areas of VIP levels ≥ 1 and 2, respectively. Higher VIP levels are labeled.

heat release. However, in other mesovortices, e.g., polar lows, tropical cyclones or lake vortices, a sizeable fraction of the low-level heating may come via sensible heat flux from the ocean or lake surface (see Forbes and Merritt, 1984; Sardie and Warner, 1985; Emanuel, 1986). Of course, in any case (latent or sensible heating or both), the positive feedback would depend upon the maintenance of the favorable environmental conditions by the larger-scale flow, e.g., moisture supply, air–sea thermal contrast, weak horizontal deformation, etc.

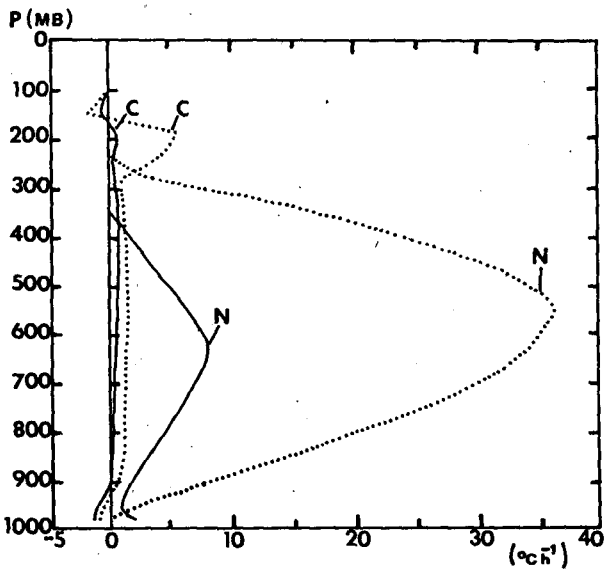

FIG. 16. Vertical heating profiles from convective (*C*) and grid-resolvable scale (*N*) processes. Profiles are taken near the center of the mesovortex. Solid and dotted lines are for the same grid point at incipient and mature stages, respectively. Note that grid-resolvable scale heating rates are instantaneous values and only occur at a model grid point for a period much less than an hour.

In the Johnstown flood case, the evolution of the mesovortex appeared to be dependent upon the depth of the low-level high-θ_e air from the west and northwest of the convective region. Note that the layer with $\theta_e \geq 345$ K became deeper as the low-level westerly jet brought high-θ_e air into the cyclonic region and as the boundary layer developed. Conversely, the depth of high-θ_e air decreased as the mesovortex moved downstream and the large convective region over western Pennsylvania intercepted the westerly flow of high-θ_e air (see Figs. 7–10). It is important to point out that the parameterized effect of moist downdrafts in convection and the subsiding branch of the mesoscale vertical circulation (Figs. 9 and 10) tended to bring lower-θ_e air from the midtroposphere into the boundary layer and help reduce the depth of high-θ_e air. The weakening of the low-level jet during the evening hours may also have helped to reduce the depth of low-level high-θ_e air. Since the increase and subsequent decrease in the depth of high-θ_e air appear to correspond with the development and decay, respectively, of the mesovortex, the moist downdrafts and the mesoscale subsidence may be natural limiting processes to the amplification

of warm-core vortices over land. Further development of a vortex may depend upon the contributions of surface fluxes (see Emanuel, 1986) and an *uninterrupted* low-level supply of high-θ_e air by a low-level jet (see Merritt, 1985). Moreover, the requirement for a sustained supply of high-θ_e air conforms to Johnston's (1981) observational findings that MCC-generated mesovortices tend to decay and eventually dissipate if they drift into air masses with lower θ_e. On the other hand, the systems tend to persist and/or redevelop if the air mass and the supply of low-level high-θ_e air remains unchanged. Although the development and maintenance of the Johnstown mesovortex appear to depend on the depth of high-θ_e air, the radius of the vortex seems to vary inversely, i.e., as the depth of the high-θ_e air increases, the vortex intensifies and contracts, and vice versa. Both of these relationships to the depth of the high-θ_e air agree with the results of Laufersweiler (1985) who performed low-order spectral studies on the response of a stratified fluid to various depths and locations of heat sources.

After large amounts of low- to midlevel moisture are brought to saturation through the positive feedback process, the potential/kinetic energy conversion and radial transport of low-level absolute angular momentum are responsible for the rapid generation of intense vorticity associated with the vortex (see Eliassen, 1952). Specifically, after about 2 h of model time, when the resolvable-scale latent heat release exceeds adiabatic cooling and horizontal transports, the remnant warming produced a large temperature gradient between the source region and its larger-scale environment. The thermal wind relationship requires an adjustment of the momentum field to such a temperature perturbation, thereby producing large tangential accelerations. Because of the weak horizontal deformation in the Johnstown MCSs environment, the available potential energy was almost localized to support this process of vorticity concentration. This process appears to be particularly important at the midlevels where maximum heating occurred. In the lower levels, the presence of the low-level jet helped the "spin up" by transporting the large angular momentum. When the relative vorticity of the generated vortex circulation became larger than the local Coriolis parameter (f), inertial stability began to play an important role in stiffening the vortex (see Schubert and Hack, 1982; Hack and Schubert, 1986). Specifically, the generated large cyclonic circulation tended to produce resistance to radial displacement of air parcels, and this prohibited available potential energy from propagating away from the heat source. This mechanism appeared to be responsible for the maintenance of the vortex properties even after 2100 UTC when only a small amount of resolvable-scale condensation occurred (see Fig. 14). The inertial stability argument can also be used to help explain the observed longevity of atmospheric vortices and associated MCCs such as that found by Johnston (1981). Note that in the present simulation, as the inertial stability increased as a result of increasing warming, the horizontal dimension of the vortex decreased. This tended to further accelerate the tangential flow.

While the resolvable-scale condensation seems to be responsible for the intensification of the mesovortex, it is extremely important to realize that it is the deep convection that is probably instrumental in modifying the environment in such a way as to create the favorable thermodynamic and dynamic conditions that permit the intensification to take place. Consider that the deepening of the mesovortex is dependent upon having a relatively strong lower tropospheric latent heat release maximum, and that this requires low-based stratiform clouds. This implies the existence of an environment that is saturated or close to saturation and has a conditionally unstable but nearly moist adiabatic lapse rate. This type of thermodynamic structure tends to evolve as a result of deep convection (see Maddox, 1983). In the present case, sensitivity tests reveal that an initial near-saturated moist adiabatic condition over Lake Erie is crucial for the generation of the mesovortex (see Zhang and Fritsch, 1986c). This initial near-saturated condition was produced by the repeated formation of deep convection as a weak short wave and associated MCSs propagated from South Dakota toward Pennsylvania during a four-day period (see Bosart and Sanders, 1981).

It should be noted, however, that even though deep convection can help create the deep moist environment suitable for mesocyclogenesis, it also acts as a brake on the rate of amplification. Two sensitivity experiments were conducted to investigate the effect of deep convection on the mesovortex. In the first experiment, deep convection was completely omitted (Zhang, 1985); in the second experiment, only cooling by moist downdrafts from deep convection was omitted (Zhang and Fritsch, 1986b). The results of both experiments indicated that the mesovortex deepened significantly more when convection or moist downdrafts were omitted. A similar result was found by Anthes et al. (1983) and Sardie and Warner (1985). In the present simulation of the Johnstown flood, a large area of deep convection occurred after 1800 UTC along the western outflow boundary upstream from the vortex. This "western" convection developed at the expense of the energy being supplied by the low-level jet that was originally feeding high-θ_e air to the vortex. Meanwhile, mid- to upper-level warming by convection and mesoscale subsidence tended to reduce the horizontal temperature gradient created by the resolvable-scale condensation, and thus contributed to a decrease in the cyclonic circulation associated with the vortex. Furthermore, the moist downdrafts from the deep convection tended to lower the equivalent potential temperature in the adjacent environment and increase lower-level static stability, thereby further slowing the deepening of the downstream vortex. This "braking" effect of the moist

downdrafts can be understood as a vertical process in which the low-level cooling and drying not only tend to stabilize the atmospheric column and raise the effective inflow to higher levels, but to remove moisture that otherwise would be used for the positive feedback processes as mentioned before. Of course, if the larger-scale energy supply from surface fluxes or from a low-level jet overwhelms the convective removal process, then it may be possible for the mesovortex to intensify. It is also important to point out that the vortex-generated low-level cyclonic circulation tends to bring lower-θ_e air from southeast of the Appalachians into eastern Pennsylvania (see ZF86), thus not only affecting the evolution of the squall line but braking further development of the vortex.

The development of long-lived, inertially stable warm-core vortices within MCCs raises many questions about cause and effect with respect to the development, structure and persistence of MCCs. For example, is the tendency for MCC cold cloud shields to assume a nearly circular shape a manifestation of a vortex developing within the system? Is inertial stability through rotation responsible for the characteristic longevity of MCCs? Certainly, inertial stability can lengthen the lifetime of a weather system (Ooyama, 1982; Schubert and Hack, 1982; and Frank, 1983) and enhance upscale and downscale interactions among the vortex circulation, synoptic environment and deep convection. It also should make MCCs more deterministic in terms of numerical prediction of their evolution. Based on the present numerical study, many different physical processes appear to affect the development, maintenance and decay of the mesovortex. The qualitative and quantitative interactions among these processes have yet to be well understood. Extensive theoretical and observational studies are strongly recommended.

6. Summary and conclusions

Through the use of a modified version of the Anthes and Warner (1978) three-dimensional mesoscale numerical model, an inertially stable, warm-core mesovortex has been examined and discussed. The vortex developed in association with the MCC that produced the 19–20 July 1977 Johnstown flood. The location and propagation of the simulated vortex correspond closely to that of a mesolow analyzed by Hoxit et al. (1978) and Bosart and Sanders (1981). The warm-core nature of the vortex conforms to the results of Bosart and Sanders (1981) in that the MCC that produced the Johnstown flood became a tropical storm as it moved over the warm water of the Atlantic. In the model simulation, the mesovortex has a space scale of 100–200 km in diameter, although the diameter of an associated anticyclonic outflow aloft is several hundred kilometers larger than that of the vortex. The duration of the vortex system is more than 18 hours. The vortex was initiated by preexisting mesoscale ascent that was produced either by deep convection prior to the model initial time or by forcing from an extratropical traveling short wave (or, more likely, by combination of both). Later, the mesovortex was supported by latent heat release from stratiform condensation in the lower to middle troposphere and maintained by the resulting inertially stable rotational flow after resolvable-scale heating diminished.

Cross sections at various stages in the life time of the mesovortex show a very intense vertical circulation with strong low-level convergence (7.5×10^{-4} s^{-1}) and upper-level divergence (10^{-3} s^{-1}). In the low- to mid-levels, wind flows accelerated as they approached the vortex and then rapidly decelerated following passage of the vortex center. The cyclonic circulation extended from the surface to 300 mb where a changeover to an anticyclonic circulation occurred. Maximum vorticity values (10^{-4} to 10^{-3} s^{-1}) occurred between about 850 and 700 mb. A pool of cool moist downdraft air developed in the surface to 850 mb layer beneath the warm core. Above the warm core, cooling by adiabatic expansion produced a cold dome in the vicinity of the tropopause (i.e., in the 200 to 300 mb layer). It is found that equivalent potential temperature and the horizontal momentum are uniformly distributed within the warm core layer. The vertical uniformity of horizontal momentum provided an important heat-preserving mechanism for the rapid generation and maintenance of the warm-core structure. At upper levels, as a consequence of potential/kinetic energy conversion, the vortex-circulation-generated-mesohigh tended to block the incoming flow ("obstacle effect") while accelerating outgoing flow (formation of jet streak).

The grid-resolvable scale condensation from mesoscale moist ascent within the MCSs made a significant contribution (30%–40%) to the total rainfall amount. The simulated axis of the heaviest grid-resolvable scale rainfall correlates well to the path of the observed mesolow. It appears that the positive feedback processes among low- to midlevel latent heat release, low-level mass and moisture convergence, and surface pressure falls, are responsible for the rapid spinup of the mesovortex through the thermal wind balance while inertial stability helps the longevity of the vortex circulation. The vortex, as well as its associated resolvable-scale condensation, weakened as 1) convective warming and mesoscale subsidence reduced the mid- to upper-level horizontal temperature gradient; 2) moist downdrafts gradually lowered the equivalent potential temperature in the adjacent environment; 3) a large area of upstream convection intercepted the low-level supply of high-θ_e air; 4) the low-level jet weakened; and 5) low-θ_e air from east of the Appalachians flowed into the vortex.

The results indicate that successful prediction of the evolution of mesoscale convective systems and significant improvement of quantitative precipitation forecasts not only hinge upon the model treatment of con-

vection, but also depend upon the physics of other mesoscale processes. In particular, the resolvable-scale phase changes, and their associated latent heat release, strongly affect the mesoscale circulation and contribute a considerable fraction of the total precipitation from the mesoscale system. Moreover, the genesis of inertially stable warm-core vortices by the resolvable-scale processes can change the behavior of the entire convective system and is possibly the dominant mesoscale *organizational* feature within mesoscale convective systems.

Acknowledgments. This work was supported by NSF grants ATM-8218208 and ATM-8418995, USAF AFOSR-83-0064, and NOAA Cooperative Agreement NA82AA-H-00027. We are grateful to L. Bosart and J. Molinari for providing the dataset for the initial conditions, to L. Giordano for making available the original radar scope tracings from the Pittsburgh radar, and to J. M. Brown for his constructive review and helpful suggestions. We acknowledge R. H. Johnson for kindly providing Fig. 12 for this paper. We also benefitted from discussions with W. Cotton, K. Emanuel, C. Leary, R. Houze, J. McBride, G. Holland, R. Rotunno and W. Frank. S. Frandsen skillfully prepared the manuscript. The computations were performed at the National Center for Atmospheric Research which is sponsored by the National Science Foundation.

REFERENCES

Anthes, R. A., 1977: A cumulus parameterization scheme utilizing a one-dimensional cloud model. *Mon. Wea. Rev.*, **105**, 270–286.

——, and T. T. Warner, 1978: Development of hydrodynamic models suitable for air pollution and other mesometeorological studies. *Mon. Wea. Rev.*, **106**, 1045–1078.

——, and D. Keyser, 1979: Tests of a fine-mesh model over Europe and the United States. *Mon. Wea. Rev.*, **107**, 963–984.

——, Y.-H. Kuo and J. R. Gyakum, 1983: Numerical simulations of a case of explosive marine cyclogenesis. *Mon. Wea. Rev.*, **111**, 1174–1188.

Barnes, G. M., E. J. Zipser, D. Jorgensen and F. Marks, Jr., 1983: Mesoscale and convective structure of a hurricane rainband. *J. Atmos. Sci.*, **40**, 2125–2137.

Bosart, L. F., and F. Sanders, 1981: The Johnstown flood of July 1977: A long-lived convective storm. *J. Atmos. Sci.*, **38**, 1616–1642.

Brown, J. M., 1979: Mesoscale unsaturated downdraft driven by rainfall evaporation: A numerical study. *J. Atmos. Sci.*, **36**, 313–338.

Chan, J. C.-L., 1984: An observational study of the physical processes responsible for tropical cyclone motion. *J. Atmos. Sci.*, **41**, 1036–1048.

Cheng, C.-P., and R. A. Houze, Jr., 1979: The distribution of convective and mesoscale precipitation in GATE radar echo patterns. *Mon. Wea. Rev.*, **107**, 1370–1381.

Cotton, W. R., R. L. George, P. J. Wetzel and R. L. McAnelly, 1983: A long-lived mesoscale convective complex. Part I: The mountain-generated component. *Mon. Wea. Rev.*, **111**, 1893–1918.

Eliassen, A., 1952: Slow thermally or frictionally controlled meridional circulations in a circular vortex. *Astrophys. Norv.*, **5**, 60 pp.

Emanuel, K. A., 1986: An air–sea interaction theory for tropical cyclones. Part I: Steady-state maintenance. *J. Atmos. Sci.*, **43**, 585–604.

Eom, J., 1975: Analysis of the internal gravity wave occurrence of 19 April 1970 in the Midwest. *Mon. Wea. Rev.*, **103**, 217–226.

Forbes, G. S., and J. H. Merritt, 1984: Mesoscale vortices over the Great Lakes in wintertime. *Mon. Wea. Rev.*, **112**, 377–381.

Frank, W. M., 1978: The life cycle of GATE convective systems. *J. Atmos. Sci.*, **35**, 1256–1264.

——, 1983: The cumulus parameterization problem. *Mon. Wea. Rev.*, **111**, 1859–1871.

Fritsch, J. M., 1986: Modification of mesoscale convective weather systems. *Precipitation Enhancements—A Scientific Challenge*, Meteor. Monogr. No. 43, **21**, 77–86.

——, and C. F. Chappell, 1980: Numerical prediction of convectively driven mesoscale pressure systems. Part I: Convective parameterization. *J. Atmos. Sci.*, **37**, 1722–1733.

——, and R. A. Maddox, 1981: Convectively driven mesoscale pressure systems aloft. Part I: Observations. *J. Appl. Meteor.*, **20**, 9–19.

——, and J. M. Brown, 1982: On the generation of convectively driven mesohighs aloft. *Mon. Wea. Rev.*, **110**, 1554–1563.

——, R. J. Kane and C. R. Chelius, 1986: The contribution of mesoscale convective weather systems to the warm-season precipitation in the United States. *J. Climate Appl. Meteor.*, 1333–1345.

Gamache, J. F., and R. A. Houze, 1982: Mesoscale air motions associated with a tropical squall line. *Mon. Wea. Rev.*, **110**, 118–135.

——, and ——, 1985: Further analysis of the composite wind and thermodynamic structure of the 12 September GATE squall line. *Mon. Wea. Rev.*, **113**, 1241–1259.

Gray, W. M., 1968: Global view of the origin of tropical disturbances and storms. *Mon. Wea. Rev.*, **96**, 669–700.

——, 1979: Hurricanes: Their formation, structure and likely role in the tropical circulation. *Meteorology Over the Tropical Oceans.* D. B. Shaw, Ed., 155–218. [Published by RMS, James Glaisher Houre, Grenville Place, Bracknell, Berkshire, RG12 1BX.]

Gyakum, J. R., 1983: On the evolution of the *QE II* storm. Part II: Dynamic and thermodynamic structure. *Mon. Wea. Rev.*, **111**, 1156–1173.

Hack, J. J., and W. H. Schubert, 1986: Nonlinear response of atmospheric vortices to heating by organized cumulus convection. *J. Atmos. Sci.*, **43**, 1559–1573.

Haltiner, G. J., and R. T. Williams, 1980: *Numerical Prediction and Dynamic Meteorology.* Wiley & Sons, 477 pp.

Houze, R. A., Jr., 1977: Structure and dynamics of a tropical squall-line system. *Mon. Wea. Rev.*, **105**, 1540–1567.

——, and A. K. Betts, 1981: Convection in GATE. *Rev. Geophys. Space Phys.*, **19**, 541–576.

——, and E. N. Rappaport, 1984: Air motions and precipitation structure of an early summer squall line over the eastern tropical Atlantic. *J. Atmos. Sci.*, **41**, 553–574.

Hoxit, L. R., R. A. Maddox, C. F. Chappell, F. L. Zuckerberg, H. M. Mogil, I. Jones, D. R. Greene, R. E. Saffle and R. A. Schofield, 1978: Meteorological analysis of the Johnstown, Pennsylvania flash flood, 19–20 July 1977. NOAA Tech. Rep. ERL401-APCL43, 71 pp.

Johnson, R. H., 1984: Partitioning tropical heat and moisture budgets into cumulus and mesoscale components: Implications for cumulus parameterization. *Mon. Wea. Rev.*, **112**, 1590–1601.

——, 1986: The development of organized mesoscale circulations within Oklahoma–Kansas Pre-STORM convective systems. *Preprints, Int. Conf. on Monsoon and Mesoscale Meteorology*, Taiwan, 100–104.

Johnston, E. C., 1981: Mesoscale vorticity centers induced by mesoscale convective complexes. M. S. thesis, Dept. of Meteorology, University of Wisconsin, 54 pp.

Kane, R. J., Jr., C. R. Chelius and J. M. Fritsch, 1987: The precipitation characteristics of mesoscale convective weather systems. *J. Climate Appl. Meteor.*, (in press).

Kasahara, A., 1961: A numerical experiment on the development of a tropical cyclone. *J. Meteor.*, 259–282.

Koss, W. J., 1976: Linear stability analysis of CISK-induced disturbances: Fourier component eigenvalue analysis. *J. Atmos. Sci.*, **33,** 1195–1222.

Kuo, H. L., 1961: Convection in conditionally unstable atmosphere. *Tellus,* **13,** 441–459.

——, and Y. F. Qian, 1981: Influence of Tibetian plateau on cumulative and diurnal changes of weather and climate in summer. *Mon. Wea. Rev.*, **109,** 2337–2356.

Kuo, Y.-H., and R. A. Anthes, 1984: Mesoscale budgets of heat and moisture in a convective system over the central United States. *Mon. Wea. Rev.*, **112,** 1482–1497.

Laufersweiler, M. J., 1985: A low-order model of uniform stratocumulus cloud layer. M.S. thesis, Dept. of Meteorology, The Pennsylvania State University, 103 pp.

Leary, C. A., 1979: Behavior of the wind field in the vicinity of a cloud cluster in the intertropical convergence zone. *J. Atmos. Sci.*, **36,** 631–639.

——, 1980: Temperature and humidity profiles in mesoscale unsaturated downdrafts. *J. Atmos. Sci.*, **37,** 1005–1012.

——, and R. A. Houze, Jr., 1979: The structure and evolution of convection in a tropical cloud cluster. *J. Atmos. Sci.*, **36,** 437–457.

——, and E. N. Rappaport, 1987: The life cycle and internal structure of a mesoscale convective complex. *Mon. Wea. Rev.*, **115,** 1503–1527.

Levy, G., and W. R. Cotton, 1984: A numerical investigation of mechanisms linking glaciation of the ice-phase to the boundary layer. *J. Climate Appl. Meteor.*, **33,** 1505–1519.

Maddox, R. A., 1980: Mesoscale convective complexes. *Bull. Amer. Meteor. Soc.*, **61,** 1374–1387.

——, 1983: Large-scale meteorological conditions associated with midlatitude, mesoscale convective complexes. *Mon. Wea. Rev.*, **111,** 1475–1493.

——, D. J. Perkey and J. M. Fritsch, 1981: Evolutions of upper tropospheric features during the development of mesoscale convective complexes. *J. Atmos. Sci.*, **38,** 1664–1674.

McBride, J. L., and R. Zehr, 1981: Observational analysis of tropical cyclone formation. Part II: Comparison of nondeveloping versus developing systems. *J. Atmos. Sci.*, **38,** 1132–1151.

Menard, R., J. Merritt and J. M. Fritsch, 1986: Mesoanalysis of a convectively generated, inertially stable mesovortex. *Preprints, 11th Conf. on Weather Forecasting and Analysis,* Kansas City, Amer. Meteor. Soc., 194–199.

Merritt, J. H., 1985: The synoptic environment and movement of mesoscale convective complexes over the United States. M.S. thesis, Dept. of Meteorology, The Pennsylvania State University, 129 pp.

——, and J. M. Fritsch, 1984: On the movement of the heavy precipitation areas of midlatitude mesoscale convective complexes. *Preprints, Tenth Conf. on Weather Forecasting and Analysis.* Clearwater Beach, Amer. Meteor. Soc., 529–536.

Miller, D. A., and F. Sanders, 1980: Mesoscale conditions for the severe convection of 3 April 1974 in the east central United States. *J. Atmos. Sci.*, **37,** 1041–1055.

Molinari, J., and T. Corsetti, 1985: Incorporation of cloud-scale and mesoscale downdrafts into a cumulus parameterization: Results of one- and three-dimensional integration. *Mon. Wea. Rev.*, **113,** 485–501.

——, and M. Dudek, 1986: Implicit versus explicit convective heating in numerical weather prediction models. *Mon. Wea. Rev.*, **114,** 1822–1831.

Ogura, Y., and Y.-L. Chen, 1977: A life history of an intense mesoscale convective storm in Oklahoma. *J. Atmos. Sci.*, **34,** 1458–1476.

——, and M.-T. Liou, 1980: The structure of a midlatitude squall line: A case study. *J. Atmos. Sci.*, **37,** 553–567.

Ooyama, K. V., 1969: Numerical simulation of the life cycle of tropical cyclones. *J. Atmos. Sci.*, **26,** 3–40.

——, 1982: Conceptual evolution of the theory and modeling of the tropical cyclone. *J. Meteor. Soc. Japan,* **60,** 369–379.

Perkey, D. J., and R. A. Maddox, 1985: A numerical investigation of a mesoscale convective system. *Mon. Wea. Rev.*, **113,** 553–566.

Rappaport, E. N., and C. A. Leary, 1985: Similarities in precipitation structure of mesoscale convective systems in the tropics and in middle latitude. *Preprints, 16th Conf. on Hurricanes and Tropical Meteorology,* Houston, Amer. Meteor. Soc., 170–171.

Rockwood, A. A., D. L. Bartels and R. A. Maddox, 1984: Precipitation characteristics of a dual mesoscale convective complex. NOAA Tech. Rep. ERL ESG-6, 50 pp.

Sardie, J. M., and T. T. Warner, 1983: On the mechanism for the development of polar lows. *J. Atmos. Sci.*, **40,** 869–881.

——, and ——, 1985: A numerical study of the development mechanisms of polar lows. *Tellus,* **37A,** 460–477.

Schubert, W. H., and J. J. Hack, 1982: Inertial stability and tropical cyclone development. *J. Atmos. Sci.*, **39,** 1687–1697.

Smull, B. F., and R. A. Houze, Jr., 1985: A midlatitude squall line with a trailing region of stratiform rain: Radar and satellite observations. *Mon. Wea. Rev.*, **113,** 117–133.

Tracton, M. S., 1973: The role of cumulus convection in the development of extratropical cyclones. *Mon. Wea. Rev.*, **101,** 573–593.

Tuleya, R. E., and Y. Kurihara, 1981: A numerical study on the effects of environmental flow on tropical storm genesis. *Mon. Wea. Rev.*, **109,** 2487–2506.

Uccellini, L. W., 1975: A case study of apparent gravity wave initiation of severe convective storms. *Mon. Wea. Rev.*, **103,** 497–513.

Wetzel, P. J., W. R. Cotton and R. L. McAnelly, 1983: A long-lived mesoscale convective complex. Part II: Evolution and structure of the mature complex. *Mon. Wea. Rev.*, **111,** 1919–1937.

Zhang, D.-L., 1985: Nested-grid simulation of the meso-β scale structure and evolution of the Johnstown flood of July 1977. Ph.D. Dissertation, The Pennsylvania State University, 270 pp.

——, and J. M. Fritsch, 1986a: Numerical simulation of the meso-β scale structure and evolution of the 1977 Johnstown flood. Part I: Model description and verification. *J. Atmos. Sci.*, **43,** 1913–1943.

——, and ——, 1986b: Impact of parameterized moist downdrafts on the numerical simulations of mesoscale convective weather systems. *Preprints, 11th Conf. on Weather Forecasting and Analysis,* Kansas City, Amer. Meteor. Soc., 364–369.

——, and ——, 1986c: A case study of the sensitivity of the numerical simulation of mesoscale convective systems to varying initial conditions. *Mon. Wea. Rev.*, **114,** 2418–2431.

Zipser, E. J., 1977: Mesoscale and convective-scale downdrafts as distinct components of squall-line circulation. *Mon. Wea. Rev.*, **105,** 1568–1589.

——, R. J. Meitin and M. A. LeMone, 1981: Mesoscale motion fields associated with a slowly moving GATE convective band. *J. Atmos. Sci.*, **38,** 1725–1750.